THE INFLUENCE OF THE HYDROLOGIC CYCLE ON THE EXTENT OF SEA ICE WITH CLIMATIC IMPLICATIONS

(Final Report)

March 1993

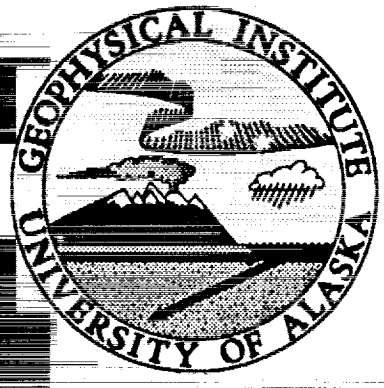

Kenneson G. Dean,
William J. Stringer,
Craig Searcy

Geophysical Institute
University of Alaska Fairbanks
Fairbanks Alaska 99775-0800

THE INFLUENCE OF THE HYDROLOGIC CYCLE ON THE EXTENT OF SEA ICE WITH CLIMATIC IMPLICATIONS

(Final Report)

March 1993

Kenneson G. Dean,
William J. Stringer,
Craig Searcy

Geophysical Institute
University of Alaska Fairbanks
Fairbanks Alaska 99775-0800

TABLE OF CONTENTS

Abstract

Multi-temporal satellite images, field observations and field measurements were used to investigate the mechanisms by which sea ice melts offshore from the Mackenzie River delta. Advanced Very High Resolution Radiometer (AVHRR) satellite data recorded in 1986 were analyzed. The satellite data were geometrically corrected and radiometrically calibrated so that albedo and temperature values could be extracted. The investigation revealed that sea ice melted approximately 2 weeks earlier offshore from the Mackenzie River delta than along coasts where river discharge is minimal or non-existent. There is significant intra-delta variability in the timing and patterns of ice melt. An estimation of energy flux indicates that 30% more of the visible wavelength energy and 25% more of the near-infrared wavelength energy is absorbed by water offshore of the delta compared to coastal areas with minimal river discharge. The analysis also revealed that the removal of sea ice involves: over-ice-flooding along the coast offshore from river delta channels; under-ice flow of "warm" river water; melting and calving of the fast ice; and, the formation of a bight in the pack ice edge. Two stages in the melting of sea ice were identified: an early stage where heat is supplied to overflows largely by solar radiation and a later stage where heat is supplied by river discharge in addition to solar radiation. A simple thermodynamic model of the thaw process in the fast ice zone was developed and parameterized based on events recorded by the satellite images. The model treats river discharge as the source of sensible heat at the base of the ice cover. The results of a series of sensitivity tests to assess the influence of river discharge on the near shore ice are presented.

Introduction

The purpose of the study described here is to investigate the processes by which arctic rivers influence the melting of sea ice. Satellite images, field observations and measurements, and river discharge records were used in the analysis. The long-range goal of the project is to understand how climate change, such as the predicted global warming, would affect river discharge and its influence on the timing of the spring melt of sea ice and its areal extent. Changes in these sea ice parameters could affect coastal water and air temperatures, and precipitation in arctic regions.

Initially, we intended to analyze both the thawing and freezing periods but for two reasons we focused on the spring thaw. First, the frequency of satellite coverage (visible and thermal wavelengths) was very limited during the ice forming period in the fall due to cloud-cover which would have greatly restricted our analysis. Second, the freeze-up process was much more complicated to analyze and to model than we initially thought. Therefore, this report will focus on the thawing process.

The report is divided into two sections. The first section describes the analysis of satellite data and field observations. The second section describes the model developed for the interaction of river discharge and its influence on sea ice.

Objectives

The overall objective of the project is to analyze the role of the hydrologic cycle and its influence on energy fluxes between the marine environment and the atmosphere in the vicinity of the Mackenzie River delta. The influence of river discharge on the albedo, thermal balance and distribution of sea ice was investigated, and a quantitative hydrologic model was developed to describe these processes in the coastal zone.

Specific objectives are:

1. to establish the morphology and position of the sea ice edge during spring melt and its relationship to river discharge;
2. to investigate the melting of sea ice and ice-edge recession related to river discharge;
3. to predict the effect of melting on sea ice offshore from rivers due to the projected global climatic warming;
4. to calculate and compare seasonal variations in energy fluxes in coastal and non-coastal areas;

5. to compare present day energy fluxes to those that may result from a climatic warming by modifying model parameters

SECTION I: ANALYSIS OF OBSERVATIONAL DATA

BACKGROUND

The thawing of rivers in the western Arctic occurs in late spring when sea ice is still largely continuous, extending from the North American coast to the Siberian coast interrupted only by relatively narrow leads and small polynyas. Melting of arctic rivers begins in the headwaters and progresses down stream. The increasing river discharge and snow melt from surrounding terrain flood the sea ice in coastal areas (Matthews and Stringer, 1984; Reimnitz, 1974). These over-ice-floods are referred to as overflows in this report. As spring progresses the relatively warm and fresh riverine water transports an increasing amount of heat from the terrestrial environment to the marine environment initiating the melting of sea ice. This heat transport results in areas of open water offshore from river estuaries before any significant melting of sea ice occurs elsewhere along the coast. The rivers also transport sediments which are deposited on the sea ice, decreasing the sea ice albedo and hence increasing solar absorption, thereby accelerating the melting of the sea ice. Fluvial transport of terrestrial heat and reduction of sea ice albedo are the dominant mechanisms for initiating the melting of sea ice.

The area offshore from the Mackenzie River delta was selected as the initial study site (Figure 1). The Mackenzie River is one of the primary sources of fresh water for the arctic basin supplying about 380 km^3/yr (UNESCO, 1978) to the Beaufort Sea and is the largest single source of sediment for the area (Milliman and Meade, 1983). Mean monthly stream flow ranges from less than 5,000 m^3/s during winter months to over 25,000 m^3/s at peak discharge in June measured at Arctic Red River (Water Survey of Canada, Yellowknife, NWT). The average rise in water level at the time of the spring peak discharge is approximately 5.5 m measured at Inuvik (Marsh and Hey, 1989).

Surface circulation in the Beaufort Sea is dominated by the anticyclonic Beaufort Gyre (Newton, 1973) but an eastward-flowing undercurrent seaward of the 50m isobath is also present (Aagaard, 1984). On the Mackenzie shelf, water mass structure and boundaries are complex with a variety of temperature, salinity and turbidity fronts that co-exist at any given time (Carmack et. al., 1989). Sources of water on the Mackenzie shelf have been quantified using the distribution of $\delta^{18}O$, salinity, temperature and nutrients (Macdonald et. al., 1989).

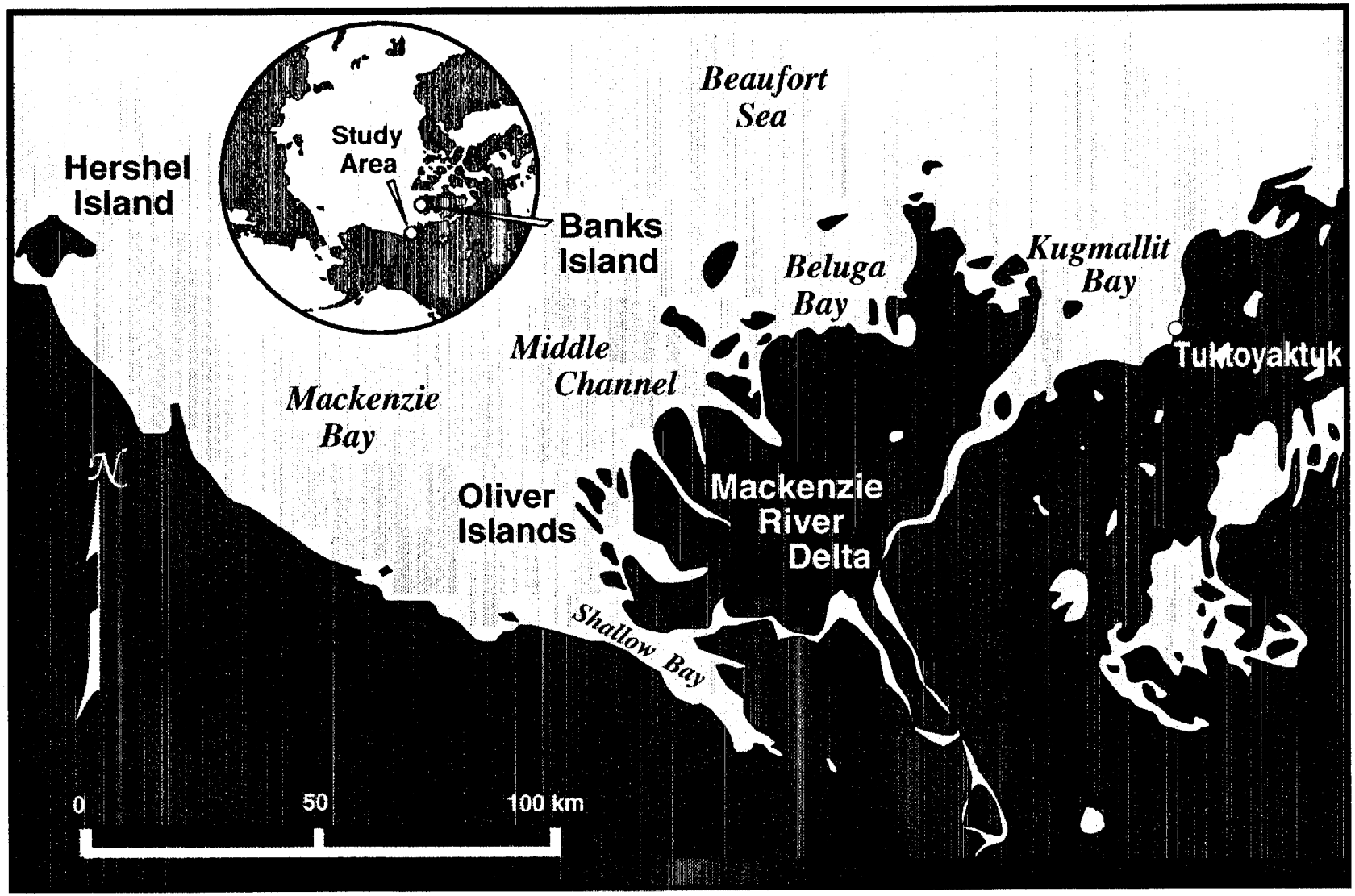

Figure 1. Location diagram of the Mackenzie River Delta and vicinity.

The Mackenzie River empties into the Beaufort Sea which has an ice cover typically from November to June, or over 60% of the time in the vicinity of the delta. From near the coast to approximately 40 km offshore, the ice that forms annually is stationary with respect to the coast by mid-winter and referred to as "fast ice". Seaward of this zone lies ice that is highly dynamic and is referred to as pack ice (WMO, 1970). When the pack ice moves away from the stationary fast ice it exposes sea water forming a lead and polynya system often referred to as the Cape Bathurst Polynya (Stirling and Cleator, 1981). When the pack ice converges, the ice is deformed into ridges along the fast/pack ice boundary parallel to the coast. Topographic relief is formed both above (ridges) and below (keels) the ice. The keels, which average 4.5 times deeper than the ridge above is high (Kovacs and Mellor, 1974), become dams trapping fresh Mackenzie water on the shoreward side (Macdonald and Carmack, 1991).

Satellite Images

Satellite imagery provides a repetitive and synoptic view of marine and terrestrial environments and an instantaneous view of dynamic hydrologic environments. The data also provide quantitative information on surface temperatures and albedo. Data from the Advanced Very High Resolution Radiometer (AVHRR) and Landsat TM sensors were used in this study. The AVHRR data were the primary source of information due to their high temporal resolution. This sensor records data twice daily with a 2200 km swath width at 1 km resolution. Data are collected in visible, reflected infrared and thermal infrared wavelengths.

Data from the Landsat TM sensor were also used by this project for detailed examinations of specific features or processes. This sensor records data with a swath width of 185 km with 30 to 120 m resolution. Repetitive coverage is recorded every 16 days, excluding side lap (Landsat 4 and 5), in visible, reflected infrared and thermal infrared wavelengths.

METHODS

Satellite Images

Several years of Advanced Very High Resolution Radiometer (AVHRR) images were reviewed to identify the year with the largest number of low cloud-cover images showing river and sea ice interactions. This search revealed 1986 as the year with the most favorable cloud conditions. Thirty-one images recorded between 25 May and 16 August were found to have low cloud cover in the vicinity of the delta and showed the temporal variability of the thaw process (see Appendix A for listing). Fifteen of the thirty-one images were selected for digital processing. Only data from the NOAA 9 satellite were purchased for radiometric consistency. Two AVHRR and a

Landsat TM digital data set were also acquired in the spring of 1991 to coincide with field observations.

The satellite data have been processed to provide quantitative measurements and qualitative interpretations. The AVHRR data were subsectioned, geometrically corrected and radiometrically calibrated using modules in the Land Analysis System (LAS) image processing software. The same modules are used to calculate temperature and albedo using equations and procedures described in the NOAA Polar Orbiter User Guide (Kidwell, 1991 and Planet, 1988). Temperature and albedo values can be read from the calibrated thermal and albedo images. These analyses were consistently applied to each image such that inter-image comparisons can be made. Land was masked on these data and a digital coastline was merged with the images to help differentiate land and marine features and for geographic reference.

The river and sea ice interactions have been analyzed using digital number (DN) level slicing techniques and the formation of color composite images. Colors were assigned to albedo and temperature ranges to form the level "slices." These slices were applied to the visible (band 1) and thermal infrared (band 4) data to quantitatively show the temporal variability of albedo and temperature values of overflows, open water, fast ice and pack ice. A standardized temperature range and color assignment was developed for the thermal data but not for the visible band data due to the magnitude of their DN ranges. Custom slices were also developed for each of the images. Color composites were formed using bands 1 (visible), 2 (near infrared) and 4 (thermal infrared) for qualitative assessment of cloud cover, sea ice and overflow conditions.

Radiometric and spatial trends between scenes were compared. Variations in albedo and temperature in fast ice, pack ice, overflows and sea surface temperatures (SST's) were analyzed as a function of time, and their areal extents were qualitatively assessed on each image.

Field Observations

Field observations were scheduled for late May, 1991 but due to an atypical spring thaw, the timing was advanced to early May. The field crew consisted of an oceanographer, a physicist/modeler, a remote sensing geologist and a remote sensing application specialist/pilot. The operation was based at the Polar Continental Shelf Project (PCSP) camp at Tuktoyaktuk, Northwest Territory, Canada. At the camp, room and board, helicopter, technical and other miscellaneous logistical support were provided.

The original plan for the field program consisted of sampling along two transects normal to the coastline from shore to the edge of shorefast ice, approximately 75 km offshore and a transect parallel to the coast along the ice edge. This operation was to be conducted during the early stages of spring breakup. A similar but more extensive program was being pursued by the Institute of Ocean Research in Sidney, British Columbia. The Canadian program was focused more on

oceanography prior to spring breakup. Fortunately, the early thaw resulted in overlap of the two field campaigns and thus we were able to use the Canadian data which more than satisfied our initial requirements. This fortunate set of circumstances permitted us to make more detailed, near-shore measurements than initially planned.

Our field program consisted of aerial observations and measurements of fast ice, sub-ice and open water marine conditions, and overflows adjacent to the coast. Aerial surveys consisted of flights over the delta in a fixed wing aircraft and the acquisition of oblique photography and vertical video recordings. The resulting observations were used to locate sites for ground sampling and for validation of satellite image interpretations. Variations in sea ice albedo and morphology were observed and mapped. Low-cloud cover AVHRR and TM data recorded in May and June were acquired to coincide with field observations as closely as possible.

Ground sampling consisted of measurements of water and ice temperature, water salinity and water depth. A transportable CTD (Conductivity-Temperature-Depth) was the primary instrument used to collect these data. A helicopter provided transportation of personnel and equipment to areas selected based on the analysis of aerial survey data. Holes were drilled through the ice and instruments were lowered into the water. Recent and ongoing measurements of offshore oceanographic conditions were incorporated in the analysis.

River Discharge Records

River discharge records were acquired from Water Survey of Canada, Yellowknife, Northwest Territory, Canada. Measurements were acquired from instruments at Arctic Red River which is the first station upstream from where the river divides into multiple distributary channels on the delta such that a reasonable estimate of discharge can be derived. The data were used to quantify the timing and volume of river discharge particularly during the break-up period and throughout the summer season. The water level and derived volumes were used to derive an annual river discharge curve on which the area of overflows and/or open water adjacent to the coast were plotted for comparison to satellite images and other field observations.

Field measurements of river water temperatures were acquired in the vicinity of Inuvik in the mid 1970's (Davies, 1975). These data were compared to satellite derived temperatures for validation. Even though over ten years separates these two data we consider the comparison very helpful.

RESULTS

Analyses of the satellite images revealed details regarding the thawing process of sea ice adjacent to and offshore from the delta, and the extent and circulation of warm and turbid water discharged by the Mackenzie River. The images also provide albedo and temperature values as well as spatial and temporal information used in a model of river-ice interactions (Section II). Variations in fast ice, pack ice, overflow position, SST's and areal extent of open water as a function of geography and time throughout the spring and summer are found on individual images. The results are discussed in chronological order and include examples of the digitally processed AVHRR satellite images that were considered to represent the thaw process. Albedo measurements were derived from visible (band 1) data and thermal measurements from the thermal infrared (band 4) data. A summary of observed thaw process features is presented in Table 1 and a complete listing of the AVHRR images cited in this report is given in Appendix A.

April and May

The April - May period is the start of the thaw process in the vicinity of the Mackenzie Delta. An image recorded on 17 April (Figure 2) shows surface conditions prior to observable melting activity and the 25 May image (Figure 2) shows the first observable thaw feature, an overflow.

The 17 April images show fast ice along the coast, the Bathurst Polynya offshore and pack ice farther seaward. No overflows were observed on the fast ice offshore of the delta. Quantitative measurements of ice albedo could not be obtained from these data due to calibration problems. General qualitative observations show ice with lower albedo offshore compared to ice adjacent to the delta. Ice temperatures well offshore were colder, less than -20° C, compared to fast ice temperatures near the delta. Adjacent to the shore, in the central portion of the delta and westward into Amundsen Bay, the fast ice temperatures were cold, -21 ° C, but slightly warmer temperatures, -17° C, were observed in the western portion of the delta (Shallow Bay) and the central portion of the delta to the lead. These warmer temperatures may be related to clouds or may be part of the thawing process. Some clouds (very likely sea smoke) were present over part of the western side of the delta. Westward trending bands of sea smoke can be seen originating from the western side of the Bathurst Polynya.

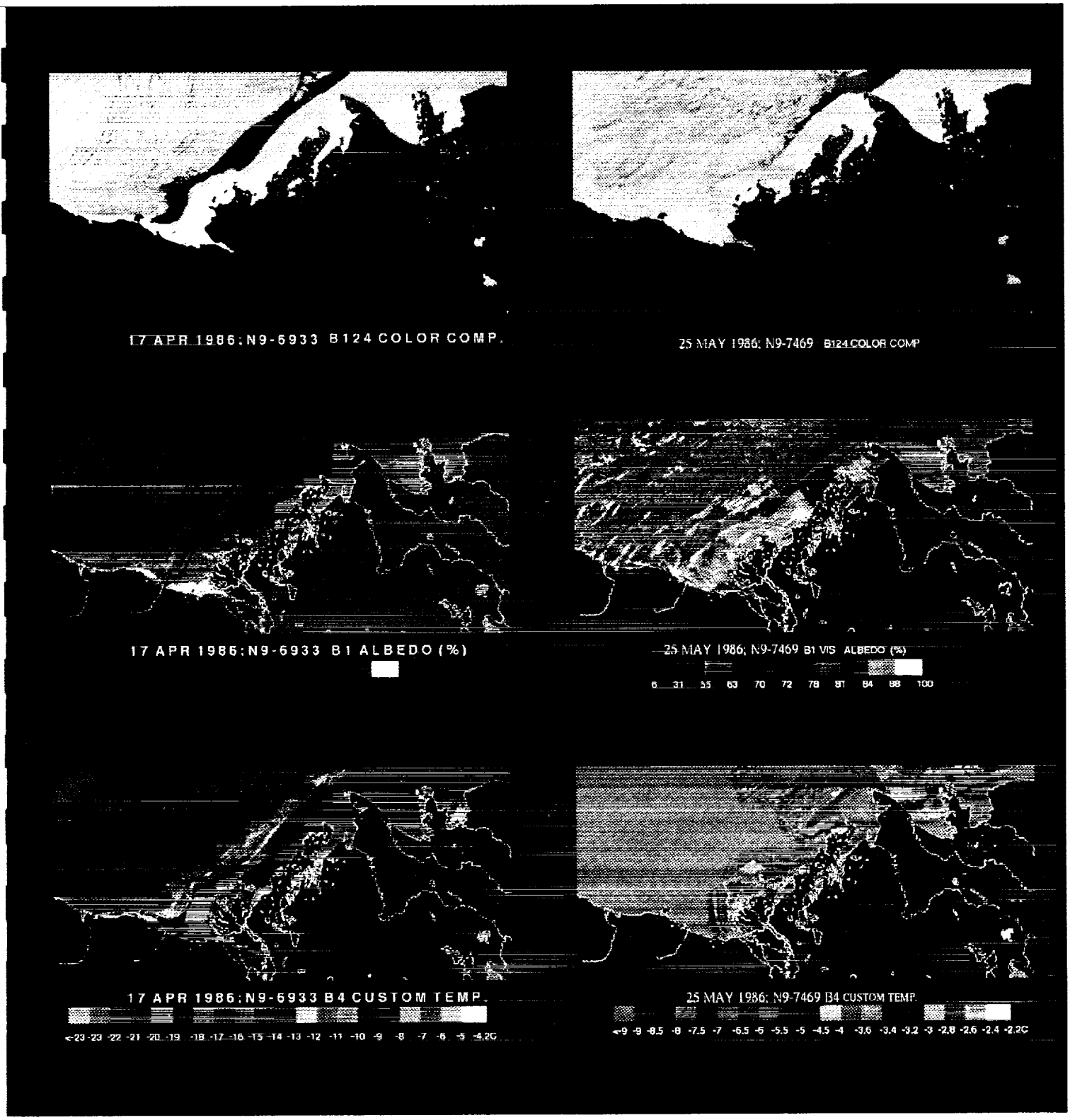

Figure 2. AVHRR satellite images recorded on 17 April 1986 (left column) and 25 May 1986 (right column). The top images are color composites using the visible (B1), near-infrared (B2) and thermal infrared (B4) bands of data. The center images are visible band data that have been color coded to show albedo. The bottom images are the thermal infrared band data that have been color coded to show temperatures.

Table 1. Date and orbit number of satellite images showing the effects of Mackenzie River discharge on sea ice. The primary feature or process that was observed on each image is described.

Date	Orbit #	Comments
17 April 86	N9-6933	No overflows observed. Ice adjacent to shore is warmer.
25 May 86	N9-7469	First overflows (four) observed immediately offshore from western discharge channels.
Early June 86		Overflows grow and coalesce (may include open water).
4 June 86	N9-7610	"Warm" water first observed beyond fast ice offshore of western channels.
9 June 86	N9-7681	Mackenzie Bight in the ice edge first appears at the western end of the lead.
22-29 June 86		Fast ice beginning to calve offshore of eastern delta channels and along the coast to the east.
3 July	N9-8020	Fast ice off of western delta channels has completely fractured forming floes. Minimal calving observed.
6 July 86	N9-8062	Fast ice and floes in western channels are mostly melted.
15 July 86	N9-8188	Remaining fast ice to the east has fractured and calved.
16 Aug 86	N9-8640	Water discharged by Mackenzie River is "warm" and turbid, and extends over 300 km to the west into the Mackenzie Bight.

The 25 May images (Figure 2) are some of the first scenes that show overflows at the mouths of delta distributary channels. These overflows are located offshore from western distributary channels that discharge into Mackenzie Bay, but few if any are offshore of eastern channels that discharge into Kugmallit Bay. Albedo measurements reveal values of $\alpha<55\%$ for overflows and 70 to 100% for sea ice. The thermal data reveal a gradient in surface temperatures ranging from -2.2 to -2.4°C in an overflow to <-7°C offshore near the lead and in the pack ice. The sub-freezing temperatures indicate that the surface of the overflow may be frozen or that clouds are affecting the signal. Clouds were present over some areas that limit analyses but a gap that might have been only semi-transparent was over most of the delta and permitted some observations. Due to the presence of clouds, the quantitative measurements are suspect. The pack and fast ice, and polynya that separates them can be seen through the cloud cover. River-water temperature measurements at this stage in 1975 were < 2 °C (Davis, 1975).

June

Break-up is very active during the June period and is characterized by the growth of overflows, calving of fast ice, some fluctuations in the position of the pack ice edge including the formation of a bight in Mackenzie Bay. "Warm" SST's can be seen off of western channels. These temperatures increase throughout the month. River-water temperature measurements at this stage in 1975 were 2 to 12 °C (Davis, 1975). Images representing this period were recorded on 4 and 14 June.

The 4 June images (Figure 3) show that the overflows have grown considerably compared to the May image and now can be seen off most distributary channels. The western channels (Reindeer and Middle) have larger and more numerous overflows compared to Eastern Channel in Kugmallit Bay which are small. The size of the Bathurst Polynya does not appear to be significantly greater than on previous images. On the visible band data the albedos of the overflows are low, 11 to 36%. The fast ice in the vicinity of the delta has an albedo as low as 36%, compared to the greater than 70% values for pack ice. Due to clouds the pack ice values may be inflated. The thermal data reveal our first observation of overflows with above zero temperatures. The temperatures of overflows and ice adjacent to the delta are 0 to 2.2°C. Seaward of the overflows the fast ice has a thermal gradient ranging from 0° C near the overflows to -2.4°C offshore near the lead. Pack ice and polynya temperatures could not be derived due to clouds.

Between 4 and 9 June the pack ice eventually moved seaward slightly but in Mackenzie Bay the pack-ice edge receded rapidly forming a bight (9 June), referred to as the "Mackenzie Bight" (Morris, 1993), offshore of the western channels. The Mackenzie Bight continued to increase in size reaching its greatest extent on 14 June. Also, some possible calving of Mackenzie Bay fast ice can be seen on the 8 and 9 June images.

The 14 June images (Figure 3) show that the seaward extent of the western fast ice is much less than on 4 June (Figure 3) and calved floes are readily apparent. The Mackenzie Bight extends farther into the pack ice. The overflows are beginning to coalesce in the western and central portions of the delta. The overflows in Kugmallit Bay are larger than on the previous image. The albedo of overflows and immediately adjacent fast ice range from 10 to 50% with lower values close to shore. Water in the polynya has the lowest albedo, 4 to 14%. Fast ice albedo ranges from 50 to 72% in the vicinity of the lead while pack ice values are greater than 72%. The temperatures adjacent to the delta range from 0.2°C for fast ice to 6.6 to 10.5 °C for overflows and/or open water. Fast ice next to the polynya has values of 0.4 to 0.6 °C. Water temperatures in the polynya range from 0.6 to 6.6°C offshore from the delta beyond Herschel Island. The edge of the pack ice is approximately 180 km offshore. Some clouds or sea smoke appear to be along the western edge of the delta, over Amundsen Gulf and well offshore over the pack ice.

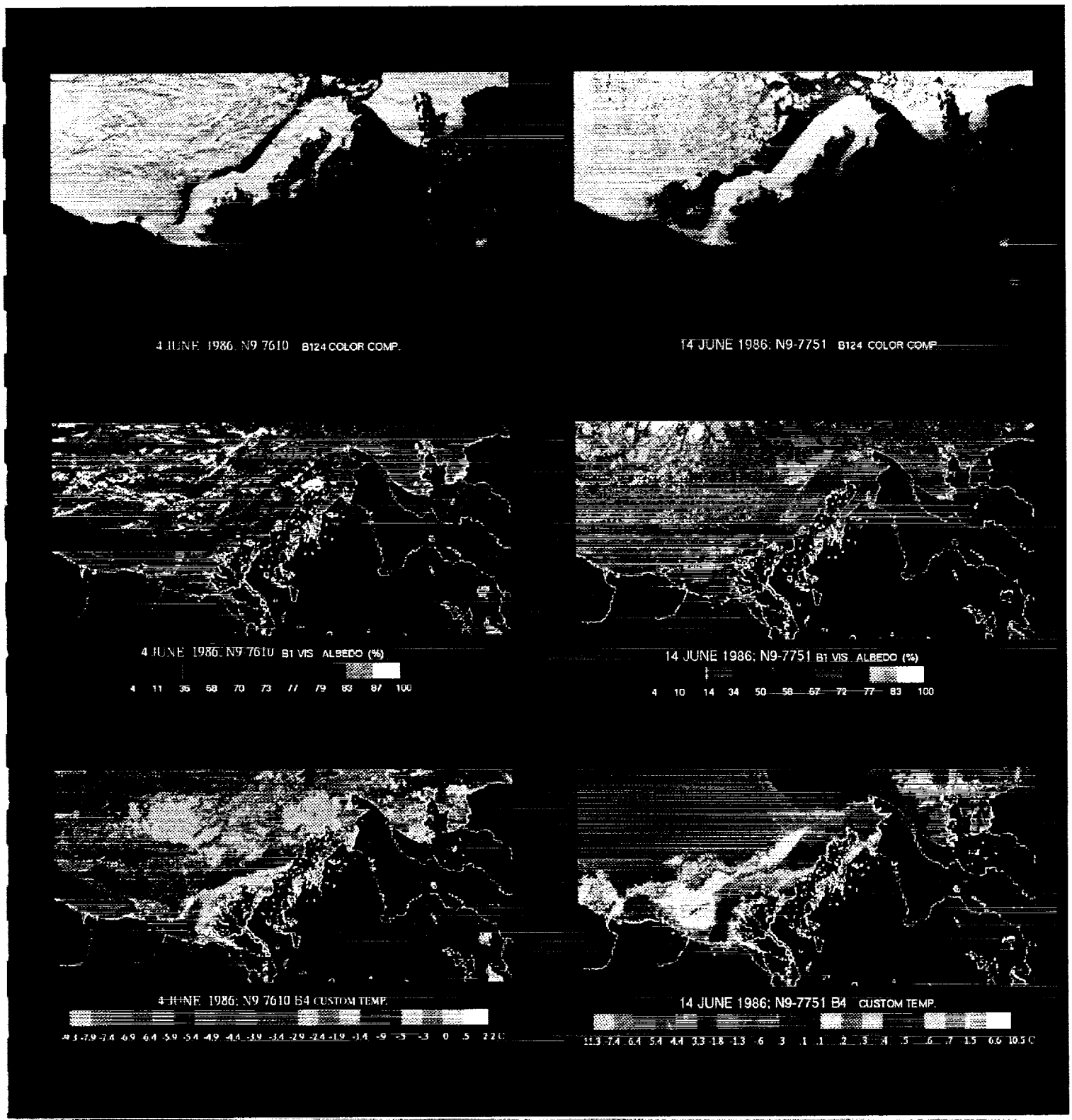

Figure 3. AVHRR satellite images recorded on 4 June 1986 (left column) and 14 June 1986 (right column). The top images are color composites using the visible (B1), near-infrared (B2) and thermal infrared (B4) bands of data. The center images are the visible band data that have been color coded to show albedo. The bottom images are the thermal band data that have been color coded to show temperatures.

The last half of June is characterized by changes in the fast ice and the Mackenzie Bight. A few floes continue to calve from the ice edge in Mackenzie Bay and are transported by currents to the pack ice edge in the Mackenzie Bight. Often these floes appear to break apart and melt before they get to the pack ice edge (14 to 29 June images). In areas east of Mackenzie Bay the fast ice starts to calve after 22 June and is most clearly evident on the 29 June image. A darkening of the fast ice along the delta coast and to the east starts on 14 June and becomes very distinct on the 29 June image. During most of late June the Mackenzie Bight ice edge remains between Herschel Island and Demarcation Point approximately 150 to 200 km from Shallow Bay.

July

Break-up activity in July consists of the removal of the fast ice, seaward extension of warm turbid Mackenzie River water from western channels and minimal movement in the position of the Mackenzie Bight. The fast ice in Mackenzie Bay has completely fractured into floes between 22 June and 3 July. By 6 July most of these western floes were either transported seaward into the Mackenzie Bight or have fractured or melted in the bay. In 1975 river-water temperatures peaked in July with values of 12 to 16 °C (Davis, 1975). The images representing this period were recorded on 5 July (Figure 4) and 12 July (Not shown).

The 5 July images show that floes in Mackenzie Bay are now mostly melted or have been transported seaward but the fast ice is only beginning to break-up to the east (Figure 4). Open water extends from the coast to the ice edge 70 km offshore except in the Mackenzie Bight where it is 150 km offshore. The Bight is partially covered by clouds but appears to be broadening. The albedo of water ranges from 3 to 25% with higher values adjacent to shore or ice floes. An isolated pocket of low albedo water, 4 to 8%, can be seen offshore from Herschel Island. Albedo of ice ranges from 25 to 56% with lower values (25 to 39%) on floes. Values greater than 56% appear to be related to clouds. Isolated pockets of warm water in bays have begun to coalesce in the western and central delta. Several pockets or tongues of warm coastal water can be seen advancing along shore to the west. To the east, "warm" water (<14°C) can be seen in Kugmallit Bay although fast ice still stretches across its entrance. Coastal water SST's peak at 14°C adjacent to the coast with SST's decreasing to 1.1°C offshore. Ice and water temperatures near the ice edge are 0.6 to 1.1°C and decrease to subfreezing temperatures in the pack ice where clouds prevent additional measurements. Fast ice temperatures are 1.6 to 2.6°C. Clouds obscure features along the western and northern edge of the images.

From mid- to late July the remaining fast ice disintegrates and the Mackenzie Bight remains relatively unchanged. The 12, 13 and 15 July images show the calving and break-up of fast ice in the eastern delta and along the coast further to the east. Most of the floes are either melted or transported seaward of the coastal region by 17 July. The 12 July images (not shown) are very

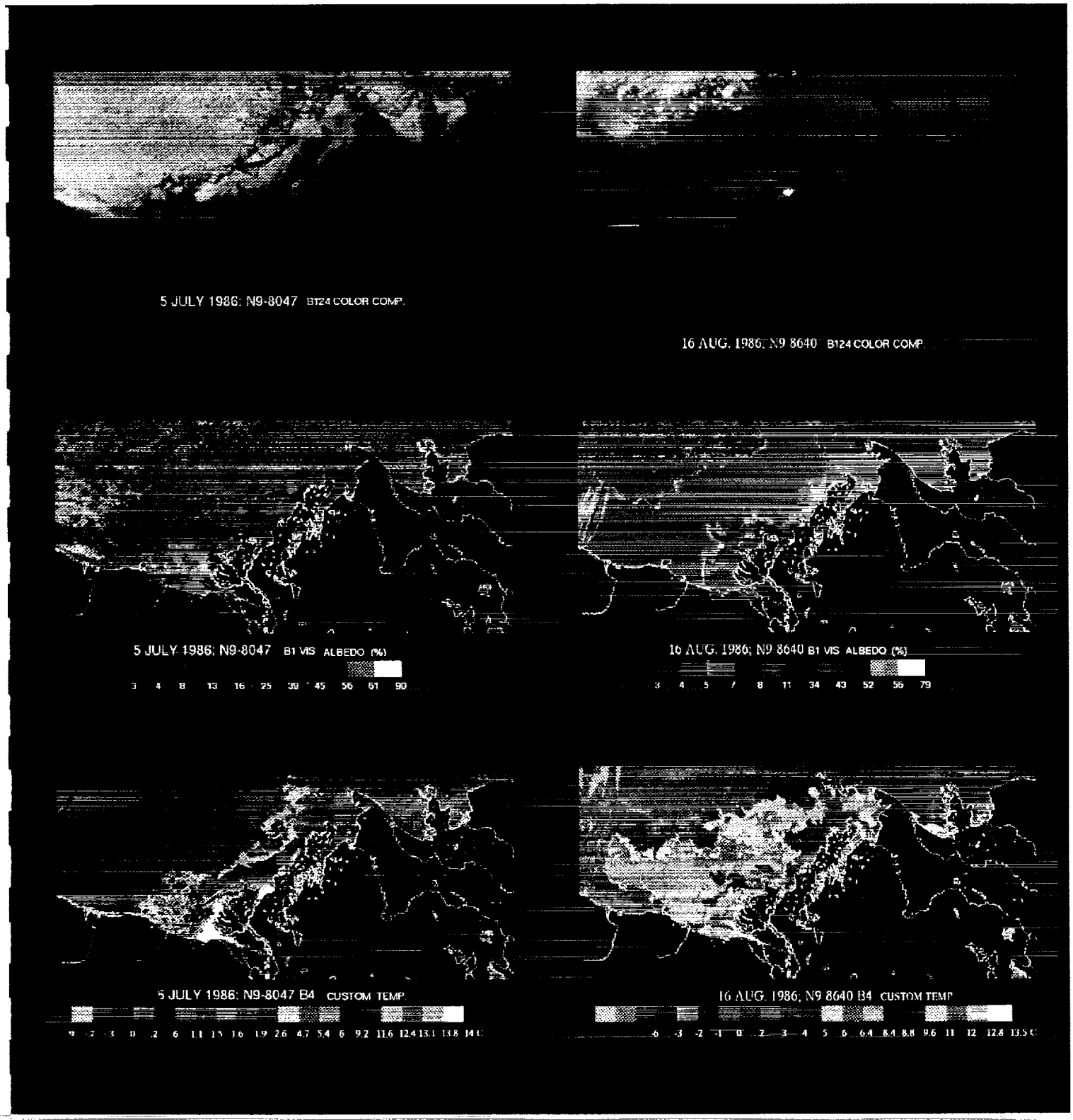

Figure 4. AVHRR satellite images recorded on 12 July 1986 (left column) and 16 August 1986 (right column). The top images are color composites using the visible (B1), near-infrared (B2) and thermal infrared (B4) bands of data. The center images are the visible band data that have been color coded to show albedo. The bottom images are the thermal band data that have been color coded to show temperatures.

similar to the 5 July image but show floes calving from the fast ice and provides a cloud-free view of the ice edge and the Mackenzie Bight. Some changes in the shape of the bight are apparent on the 22 July image.

August

By August most, if not all, of the ice is melted in the vicinity of the delta and break-up is completed. "Warm" water discharged by the Mackenzie River can be seen hundreds of kilometers west of the delta in the Mackenzie Bight. In late July and early August (1986) the delta area was mostly cloudy but observations on 4 to 16 August show that the pack ice has moved offshore. In 1975 measured river-water temperatures begin to decrease in August from 16 to 10 °C (Davis, 1975).

The 16 August images (Figure 4) show sea ice away from the Alaskan and Canadian coasts west of the delta. Turbid water from the Mackenzie River is more distinct on this image compared to previous ones. The Mackenzie Bight in the ice edge is now near the western edge of the study area, approximately 350 km from the delta. North of the delta the ice edge is almost 200 km away. Few if any floes can be seen in the open water and the ice edge is highly crenulated with many calved floes along it. Albedo values of water range from 34% adjacent to the coast to 3% offshore. High albedo water extends along the delta coast from Shallow Bay to Kugmallit Bay. The albedo of pack ice ranges from 34% near the ice edge to 52% farther north. Warm water discharged by the Mackenzie River extends several hundred kilometers east and west of the delta with the warmest water to the west in the vicinity of the Mackenzie Bight in the pack ice. SST's range from 13.5°C adjacent to shore to 2 to 4°C near the ice edge. Ice temperatures range from 2 to -1°C. Some clouds are located along the western and northern edge of the area with those to the north extending southward over the pack ice near the image center. Water west of the delta is warmer by a factor of two compared to water east of the delta.

Field Observations

Field measurements were acquired at nine stations offshore from the Mackenzie River delta on 14 and 15 May 1991 (Figure 5). Weather conditions on 14 May were calm and overcast with air temperatures from 0.5 to 1.0°C. Data were collected at stations one through seven on this day. On 15 May the weather was clear and sunny with air temperatures at 4°C. Data were collected at stations eight and nine on this day.

The field measurements found that the floating ice thickness was approximately two meters, water temperatures were near 0°C including overflows, and that salinity measurements were approximately zero indicating that the source of the water is the Mackenzie River rather than

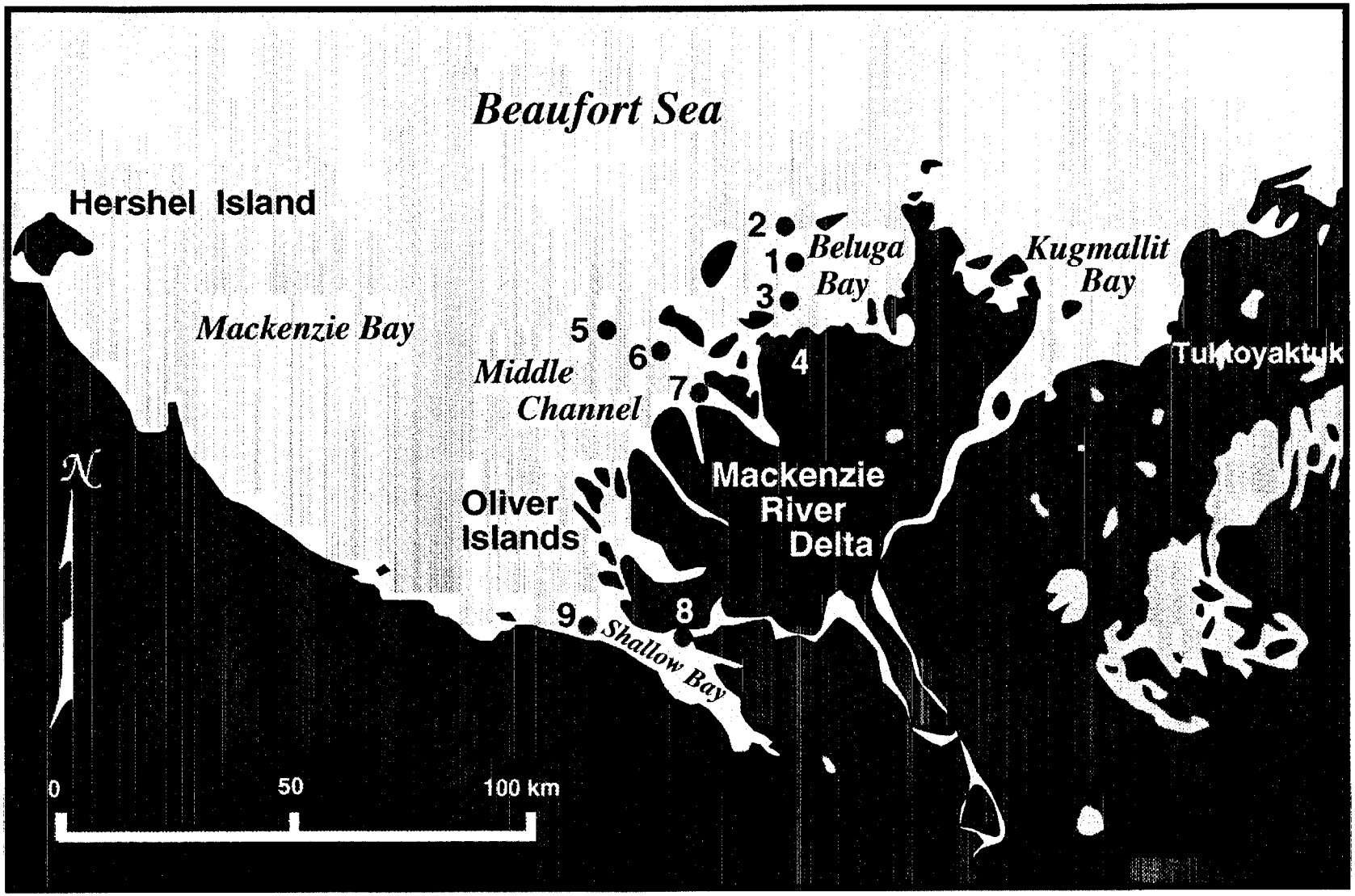

Figure 5. Location diagram of field sample sites.

marine (Table 2 and Figure 6). Measurements were taken of the water column but at two sites the water was too shallow for the CTD as indicated by water depths less than 0.5 meter. Overflows were usually measured from a hovering helicopter. At stations 8 and 9 in Shallow Bay, the ice surface was slush and a strong seaward current was present that nearly prevented the retrieval of the CTD after it had been lowered under the ice edge. Also, approximately two miles north of station 9 a pressure ridge system was observed. The ridges were 2 to 5 meters high, approximately 50 m long and aligned parallel to shore but eventually curving to the south along the mouth of the channel in Shallow Bay.

DISCUSSION

The thawing of sea ice was analyzed based on 1986 time series of AVHRR satellite images with as high temporal resolution as possible, sometimes including multiple images per day. Figures 2, 3 and 4 are examples of this data. (See Appendix A for detailed list of the images). Results from this analysis have been summarized on a series of schematic diagrams (Figure 7). These diagrams show, as a function of time; the development of overflows in May and June, the formation of the Mackenzie Bight in the western pack ice edge in early June; contiguous fast ice that has completely broken into floes in the western delta (Mackenzie Bay) by early July and fluctuations of a few tens of kilometers in the position of the pack ice edge prior to July 12 after which it eventually recedes seaward to its 16 August position. We propose that the overflows, disintegration of fast ice offshore of delta channels, and the formation of Mackenzie Bight are strongly influenced by river discharge, and that most of the effects occur earlier offshore of the western channels in Mackenzie Bay than in Kugmallit Bay and other coastal areas in this vicinity.

Overflows

Sea ice along the delta begins thawing in May in areas where river water flows over fast ice at the mouths of distributary channels. These overflows develop when sea ice is frozen to the bottom and has left only small sub-ice stream channels (Barnes et. al., 1976; Mathews and Stringer, 1984). The increased volume of water discharged by the river is greater than the capacity of the channels and hence water is forced to lift the ice or flow on its top. Since the ice is frozen in to the bottom in shallow regions it resists being lifted and hence water flows on top and seen as overflows. High sub-ice, hydrostatic pressure in the Mackenzie delta area is indicated by a small geyser on a figure by Macdonald and Carmack (1991, p. 45).

Table 2. Results from field measurements.

Station # and Conditions	Water Depth (m)	Ice Thickness (m)	Water Temp. (°C)	Salinity (ppt)	Turbidity
14 May 1991					
1. Bore hole	2.6	2.2	-0.01	0	
1a. Overflow	20 cm		0.1		
2. Bore hole	4.8	2 - 2.5	0.0 @ 0 to -0.01 @ 3 m	0.0 @ 0 to 0.2 @ 3 m	Clearest water obser. on 14 May
3. Overflow	< 0.5		0.0		Turbid
4. Hovering helicopter	1		0.2	0	
5. Bore hole	4.2	2 - 2.5 (est.)	0 @ 0 to -0.01 @ 4 m	0.0 @ 0 to 0.15 @ 4 m	Turbid
6. Hovering helicopter	< 0.5		0.2		Turbid
7. Overflow			0.7		Turbid
15 May 1991					
8. Bore hole	7	1.8	0.24 @ 0 to 0.07 @ 6 m	0.09 @ 0 to 0.1 @ 6 m	Fairly Clear
9. Bore hole	8.5	2.5	0.06 @ 0 to 0.02 @ 7 m	0.05 @ 0 to 0.13 @ 7 m	Fairly Clear

Fast Ice

Fast ice disintegrates offshore from western delta channels in Mackenzie Bay much sooner than along other coasts. The satellite images show that fast ice forms a band parallel to the coast approximately 50 km offshore. In May and early June, 1986, the shape and position of the edge of the fast ice remains stationary while the edge of the pack ice begins to fluctuate as the Bathurst Polynya opens and floes move from the pack ice into the polynya. Wind is the suspected agent for this drift. Satellite images recorded the receding fast-ice edge in Mackenzie Bay starting on 13 June when floes begin to calve from the ice (N9, 6/13/86, Orbit 7737; and on 6/14/86 Orbit 7751). The floes are transported rapidly to the northwest into the Bight (See section on Mackenzie Bight) and begin to break apart and melt as they move. The calving continues until most of the ice is removed from Mackenzie Bay on 5 July (Figure 4).

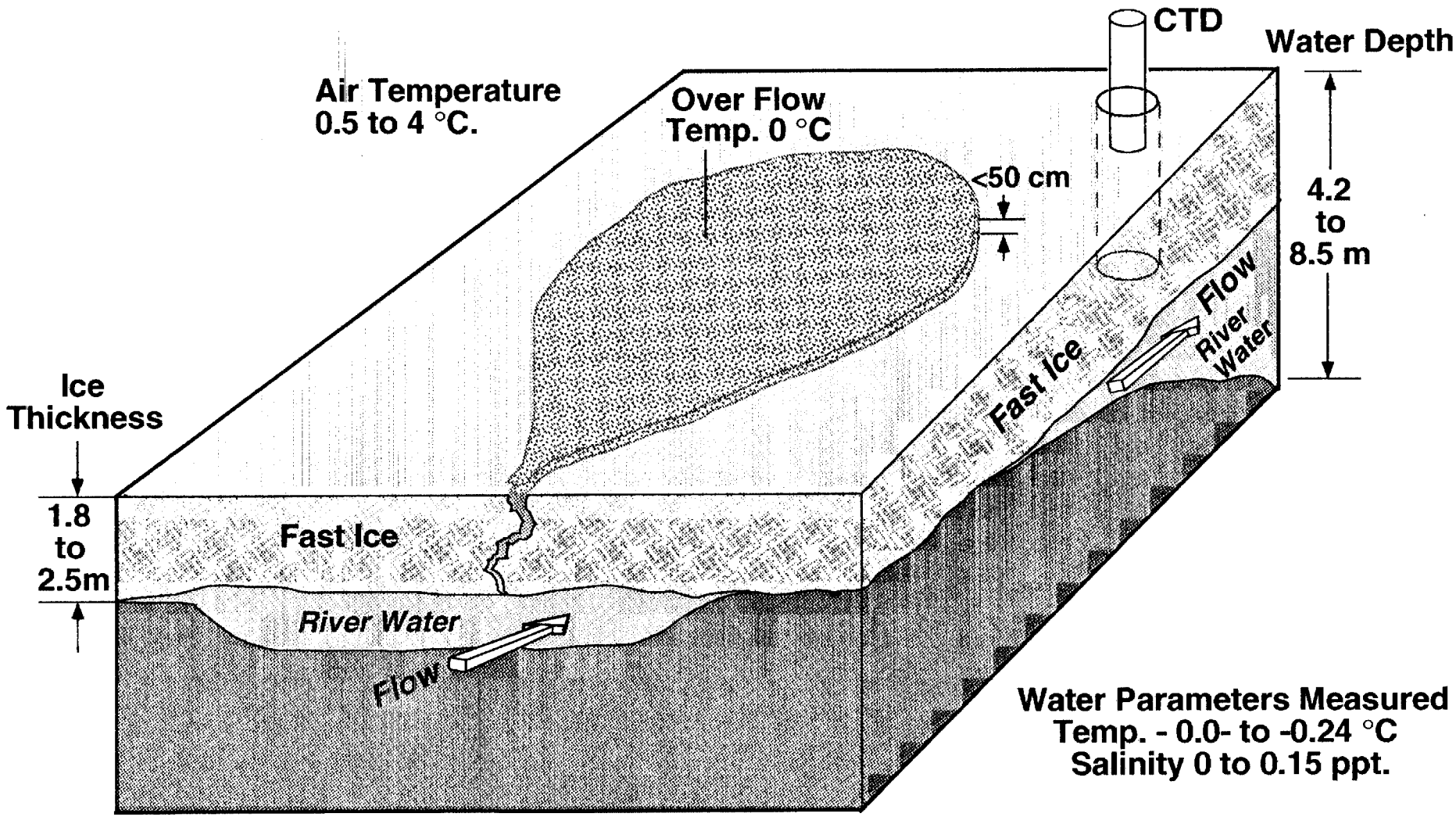

Figure 6. Schematic diagram showing results of field observations and measurements.

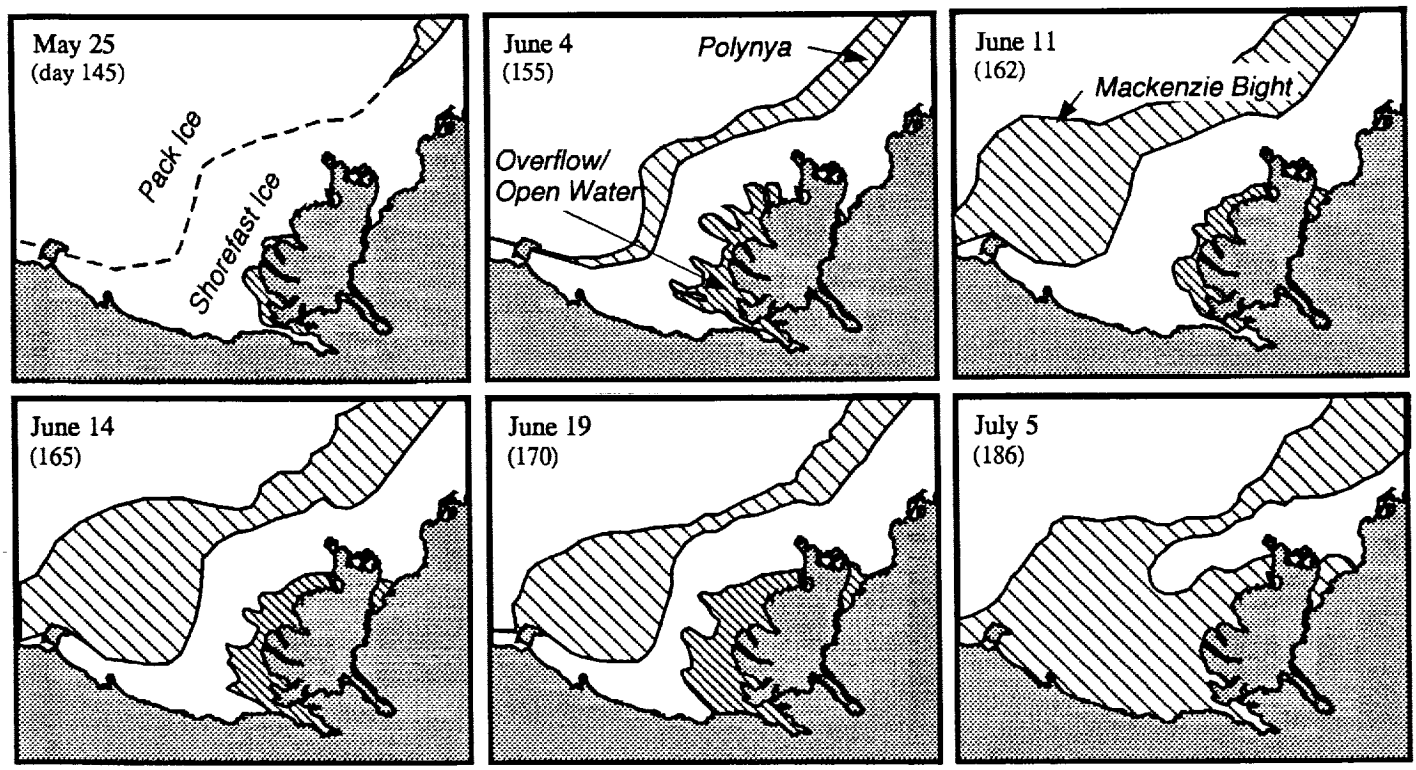

Figure 7. Schematic diagram of the Mackenzie Delta region derived from the 1986 visible band images. This sequence depicts the development of the polynya system separating the fast ice from the pack ice as well as the river-induced melting immediately adjacent to the coast. The period represented is spring breakup with the image scenes beginning on May 25 (day 145) to July 5 (day 186).

Fast ice east of Mackenzie Bay, including that portion of the delta and coastline 300 km to the east, does not begin to seriously calve until approximately 29 June (N9, 6/29/86, Orbit 7963), two weeks later than in Mackenzie Bay. Most of the fast ice has broken into floes by 13 July, about a week after the Mackenzie Bay ice. During the 5 to 15 July period a very large number of floes can be seen in the open water. These floes appear to move slowly, both seaward (north) and to the northwest towards the Mackenzie Bight compared to those in Mackenzie Bay. The floes also fracture and melt at a slower pace than those in Mackenzie Bay. The acute calving period was not observed in Mackenzie Bay possibly due to the influence of river discharge.

We did not expect to see this intra-delta variability in the timing of break-up and are surprised that fast ice along the eastern delta decays at the same time as ice in areas with minimal influence by river discharge up to 300 km to the east. Discharge measurements show that the East Channel drains into this area transports only 18% of the Mackenzie River water as measured in August of 1992 by the Water Survey of Canada (personal comm., 1993, S. Fafassnacht, Yellowknife and W. Hanna, Inuvik). This suggests that discharge from eastern Mackenzie channels is relatively low.

The Mackenzie Bight

Possible causes for the formation of the Mackenzie Bight include the melting and mechanical fracturing of ice that may result from warm Mackenzie River water, movement of pack ice along the coast to the west, tidal energy enhanced by the Mackenzie Canyon (Morris, 1993), upwellings associated with winds (Hakkinen, 1986), ice edge eddies (Johannessen et. al., 1987), or bathymetrically steered currents. The Bight is not a feature unique to 1986 but is often observed as shown by Morris (1993).

Based on our analysis of 1986 satellite images we propose that the Bight results primarily from melting of the ice by water discharged from the Mackenzie River. On the 4 June 1986 image (Figure 3) a small pocket of warm water (0.5 to 2.2°C) can be seen in the recently opened Bathurst Polynya in Mackenzie Bay. This warm water appears prior to the formation of the Bight on 9 June at a location just west of the warm water as recorded on satellite image (N9, OB 7681). The ice edge in the Bight rapidly retreats to the west by 13 or 14 June (recorded on satellite images N9, OB 7737; N9, OB 7751). Later images, e.g., 16 August (Figure 4), show warm water extending from the Mackenzie River delta to the Bight then located 350 km to the west. Also, as previously described, fast ice is removed in this area earlier than to the east (See Section on Fast Ice) where there is much less "warm" Mackenzie River water.

Additional observations suggest that the Bight forms down current from the Mackenzie River delta again supporting the hypothesis. Successive images in June and July (e.g., N9, 6/13/86, OB 7737; and N9, 6/14/86, OB 7751) show floes calved from fast ice in Mackenzie Bay

and moving westward towards the Mackenzie Bight. These floes appear to get smaller as they are presumably transported, mechanically break up, and melt. Field measurements in 1991 indicate the presence of a strong northwest-flowing current in Shallow Bay southeast of Mackenzie Bay. These observations indicate that the Mackenzie River water flows westward into the Bight enhancing or causing its formation through thermal erosion. Wind may, in part, be responsible for the westward movement of floes.

It is possible that large-scale movement of the pack ice to the west along the coast could also account for the Mackenzie Bight. The high rate of recession on 13 and 14 June could result from offshore or clockwise rotational movement of the Beaufort Gyre, which would be manifested as a lead or opening in the area of Herschel Island due to the presence of open water to the east and movement away from shore. However, significant movement of pack ice along the Alaskan coast is not obvious when comparing floes on successive images. Precise image analysis techniques need to be applied to these data, such as image registration and the generation of an animation sequence to fully investigate the details of the processes involved in the formation of the Bight.

Evidence supporting or discounting the influence of enhanced tides in Mackenzie Canyon, bathymetrically steered currents, ice edge eddies or wind driven upwellings are not definitive on the images. The Bight appears to form and enlarge near the coast instead of offshore in the vicinity of the canyon. No unusual surface manifestation relating to eddies or upwellings that can not be attributed to river discharge were observed on the images. However, to evaluate the influence of these factors measurements in the water column should be performed.

River Discharge

The Mackenzie delta appears to have undergone a transition from a steady discharge of water divided among eastern and western channels to dominance by western channels over the past 20 years. The discharge of water by the channels on the delta was thought to be evenly distributed in 1974 (Davies, 1975). More modern measurements by Canadian engineers from Environment Canada, NWT now indicate that the majority of discharge (approx. 80%) is from the western channels, predominantly the Middle and Reindeer Channels (personal comm., 1993, S. Fafassnacht, Yellowknife and W. Hanna, Inuvik). If the 1974 observations are correct then changes in channel flow, sedimentation and deposition have affected the hydrology and modified discharge into the Beaufort Sea since 1974. The extent and timing of sea surface temperature and turbidity patterns offshore from the western channels indicate that the change in the delta (if one occurred) took place prior to 1986.

Radiation Transfer Estimates

Sea ice greatly restricts the absorption of solar energy by underlying water. Thawing of ice exposes the water to the atmosphere thus significantly increasing the absorption of solar energy. In addition, the higher levels of heat and moisture exchanges between the water and the atmosphere may warm the surrounding coastal region and increase precipitation. We hypothesize that an increase in the area of the exposed sea surface or lengthening of the time that the sea surface is exposed to the atmosphere is strongly influenced by rivers and will increase the exchange effects.

To assess exposed water effects, the heat flux was approximated and compared in areas offshore of the delta, along the coast east and west of the delta (Figure 8), and far to the east adjacent to Banks Island (not shown in Figure 8). The approximated heat flux is based on the average albedo values of each area with values derived from the time sequential visible and near infrared bands of the satellite images. The results are shown as plots of albedo versus time (Figure 8). The lower curve in each graph is the average albedo of water and ice in the delta region and the upper curve is the average albedo from mostly ice in the coastal regions where minimal river discharge occurs. These data show that the albedo in thawed zones offshore from deltas (lower curve) is lower than other areas along coasts with minimal or no river input (upper curve). The integrated area bounded by each curve is proportional to the total absorbed energy per unit area over the breakup season. Since the solar radiation is assumed to be equal for each site, the difference between these two curves (represented by the shaded region) will be representative of the additional energy gained by the lower-albedo delta region. The integration shows that 30% more of the visible wavelength energy and 25% more of the near-infrared wavelength energy is absorbed by ice and water offshore of the delta compared to coastal areas with minimal river discharge.

Heat Flux and the Melt Process

We propose that the melting of ice offshore from the delta is a two stage process involving solar warming in May and warm river water in June. As is to be expected, surface temperatures increase as the season progresses. Overflow temperatures rise from approximately 0°C in late May to a few degrees above zero in early June. Field measurements in mid May of 1991 generally found the overflows a few tenths above 0°C and that river water flowing beneath the ice was within a few hundredths of 0°C, but often below zero.

The overflows decrease the albedo to as little as 1/7 of the initial fast ice value as measured from the satellite images. The decrease in the albedo results in an increase in the heat flux due to the absorption of solar energy thus providing some heat to melt sea ice. Throughout May and June the surface area of the overflows increase and thus again increases the heat flux (Figures 2 & 3). Even

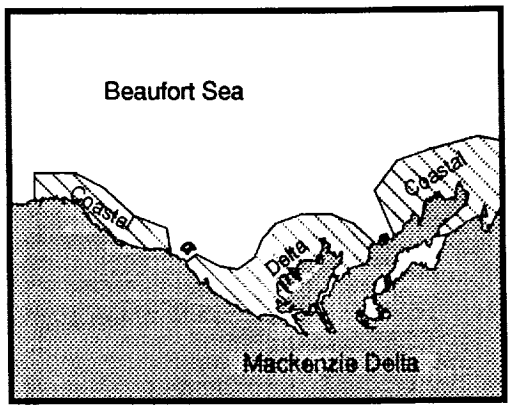

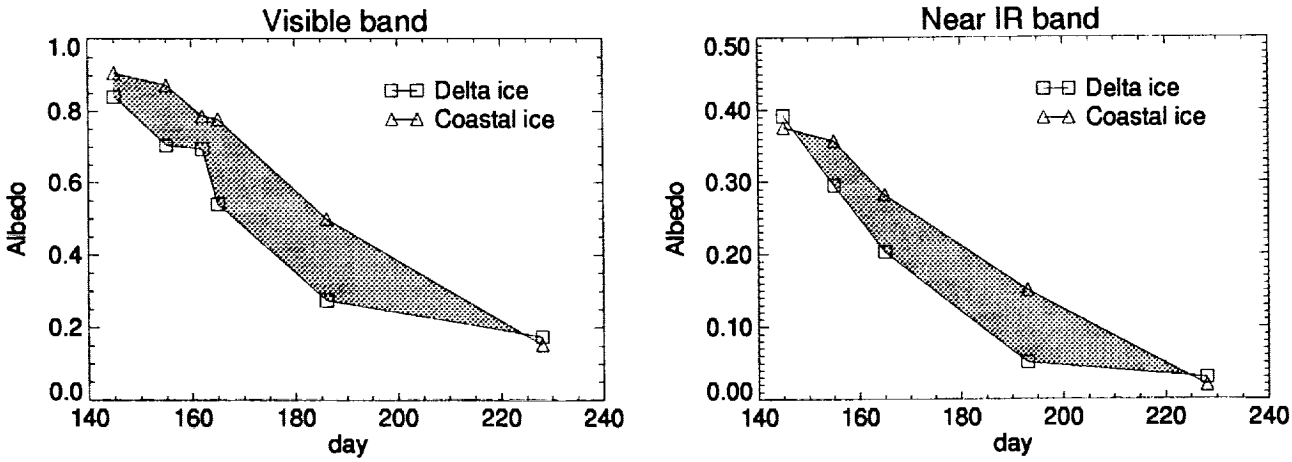

Figure 8. Average albedo measurements for the regions defined in the schematic (upper figure) in the visible (lower left) and near-IR (lower right) bands. The Delta ice region is consistently lower in albedo and hence absorbs more shortwave radiation than other coastal areas.

though this difference is small, it appears that the overflows were adding heat while river water beneath the ice contributed little energy and may have been actually taking heat away from the ice.

The albedo of fast ice in areas not affected by overflows also decreases to as little as 1/3 of the initial values again increasing the heat flux as the season progresses as seen by comparing the May data to the July data (Figures 2 & 4). This change is attributed to melt ponds that form when surface snow and ice thaw (Stringer, Univ. of Alaska, in preparation). The decrease in fast ice albedo due to snow melt is less than that found for overflows and occurs perhaps two weeks later. Thus, the overflows have a higher rate of heat flux at any stage of the ice removal compared to regions affected by melt-ponds. This difference is most pronounced in the early stages of ice-removal when overflows develop rapidly and extensive snow melt has not yet occurred.

Energy contributed by river discharge becomes the dominant source of heat used to melt ice in early June, melting fast ice and some pack ice. In Mackenzie Bay relatively warm river water can be seen on the 4 June image with SST's up to 2.2°C which is a few days after the peak water level of the Mackenzie River as measured by the Water Survey of Canada. This indicates that "warm" river water is flowing beneath the fast ice by this date. SST's rise after 4 June to as high as 14°C on 5 July. The increasing SST's for June parallels the 1974 Mackenzie River temperature profile (Davies, 1975). Thus in early June river water appears to become the dominant contributor of heat, at least offshore of western channels in Mackenzie Bay, as seen by the rise of SST's viewed on the satellite images, and melting of fast ice in June.

CONCLUSIONS

In 1986 sea ice offshore from the Mackenzie River delta melted 2 weeks earlier than along other portions of the coast where river discharge was minimal. Surprisingly, intra-delta variability affecting the sea ice is significant with earlier melting occurring offshore from western Mackenzie River channels compared to eastern ones. Melting by discharged "warm" river water primarily affects fast ice but a bight forms in the pack ice in Mackenzie Bay down-current from the western channels. We conclude that the bight develops, at least in part, due to melting of pack ice by Mackenzie River water.

Disintegration of sea ice involves: over-ice-flooding along the coast offshore from river delta channels; coalescing of these flood waters; sub-ice flow of "warm" river water; melting and calving of the fast ice; and the formation of a bight in the pack ice edge. The melting of the sea ice involves two processes; absorption of solar radiation by flood waters and warm water discharged by the river. Absorption of solar radiation is an important component of the heat flux during the initial stages of melting due to its low albedo. However, this becomes subordinate when warm river water reaches the delta and can flow freely beneath the ice. The early exposure of coastal

water offshore of the delta provides 25 to 30% additional energy absorbed by the water column affecting local and possibly regional climates.

Additional studies describing ice formation in the fall of the Mackenzie River delta are needed as well as other investigations of the freeze/thaw processes in the vicinity of other river deltas. The use of SAR images may provide information regarding ice frozen to the bottom in the vicinity of deltas where only fresh water is present and perhaps increase temporal resolution. The work on the Mackenzie River delta has revealed the presence of a high temporal image collection that could be animated to provide a better understanding of surface interactions during the melt period.

SECTION II: RIVER-ICE INTERACTION MODEL

The purpose of this section of the report is to describe the numerical model of the interaction of river discharge with sea ice. The model was developed based on the qualitative observations and quantitative measurements derived from satellite images, field data and river discharge records described in section 1 of this report.

INTRODUCTION

Previous studies (Semtner, 1984; Micklin 1981; and Aagaard and Coachman, 1975) have investigated the relationship between the Arctic Ocean freshwater budget and the stability of the upper water column and their effect on the sea ice cover. These studies were initiated in response to earlier (1970's) proposed Soviet river diversions for agricultural purposes, however, the results were inconclusive and even contradictory. While the Arctic basin may or may not be particularly sensitive to the overall freshwater budget, arctic rivers and streams do supply a significant source of sensible heat to the nearshore region. Coastal regions receiving river discharge show significant ice recession in advance of other areas along the coast, presumably as a result of this introduced heat. As long as it is in place, the near shore ice cover acts as an insulating barrier between the marine environment and the atmosphere and hence influences local climate. Alterations to the volume or timing of river discharge due to possible climatic warming could have a pronounced effect on the timing and areal extent of the degradation of the ice cover.

The satellite images, described in the previous section, are used to establish the areal extent of the ice cover and the timing of certain breakup events. This data set becomes the basis for a thermodynamic sea ice model attempting to parameterize the convective heat transfer from the river discharge to the base of the ice cover. The model also includes a surface heat balance with short and longwave radiation as well as sensible and latent heats. Such a model predicts the removal of

the ice cover as a result of thermal forcing on the two horizontal surfaces. See Appendix B for the model code.

Breakup Dynamics

The Mackenzie River discharges onto a shallow continental shelf extending 60 to 80 km offshore. At the shelf break, extensive ridging occurs during the winter as the pack ice moves laterally against the fast ice in a "shear zone". In late winter, an annually recurrent polynya (Bathurst Polynya) develops here and separates the pack ice from the fast ice.

The ridged ice in the shear zone occurs at about the 20 meter isobath and creates large-scale under ice topography which effectively separates the shelf water from the Arctic Ocean (Macdonald and Carmack, 1991). Over winter, the Mackenzie River maintains a relatively large discharge (~3,500 m^3/s) which pools on the near shore side of this ice-ridge system since the fresh riverine water is buoyant compared to the relatively saline shelf water and is effectively dammed by the keels of the shear ridges. The wintertime discharge is sufficient to maintain a consistent salinity structure and replenish the supply of freshwater as the ice is formed. Peak discharge (~30,000 m^3/s) occurs in early June but doesn't appear to have a significant effect on the shelf salinity profile except for near the ridging where a deepening of isohalines occur as the riverine water flows underneath the hanging-dam structure.

A series of generalized schematic diagrams derived from the visible band satellite images recorded in 1986 show the ice breakup process in the delta (Figure 7). The area of open water increases as the summer progresses due to the opening of the Bathurst Polynya and the melting of sea ice. The area of water immediately adjacent to the coast was measured from these images and is plotted in Figure 9 (data points). Superimposed on this figure is the discharge curve (dashed line) for 1986. Note that the first three area calculations (May 25, June 4, and June 11) are related to the discharge curve by peaking and receding in similar fashion. The thermal images for these three dates show the water to be nearly isothermal with the ice cover. Since the water and ice are assumed to be in equilibrium at the freezing point and the measured area of water receded after the peak in discharge; thereby exposing ice, it is interpreted that these are largely flooded areas. After this point, subsequent areal measurements diverge from the discharge curve. Thermal images during this period show the water warming above the freezing point and it is clear that these are areas of open water developing as the ice cover is melted laterally away from the coast.

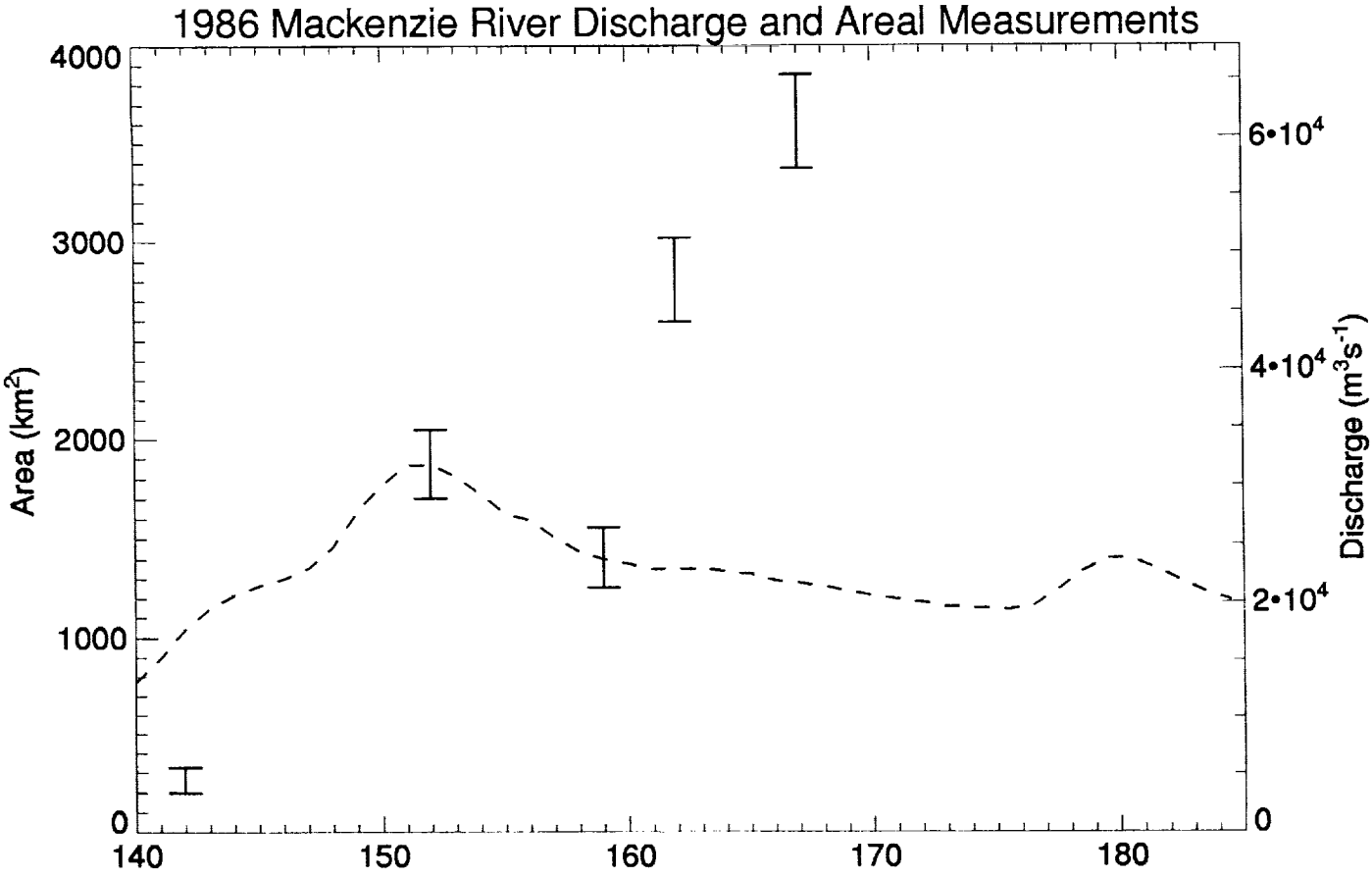

Figure 9. Comparison of 1986 Mackenzie River discharge to areal measurements of river-induced open water. The dashed line is the discharge curve ($m^3 s^{-1}$) while the data points are a calculation of the overflow or open water areas (km^2) immediately adjacent to the coast. The area of open water is derived from digitally processed AVHRR satellite images. The first three data points follow the discharge and for the most part represent overflows on top of the ice while the later points diverge as the area of open water enlarges as the ice cover recedes from the coastline.

THE RIVER-ICE INTERACTION MODEL

In the model, we consider only those changes in the near shore ice due to the thermal forcing appropriate for the arctic spring beginning around late May and continuing to mid-July. Other processes such as advection and internal stresses are ignored. Heat fluxes on the upper and lower horizontal surfaces of the ice cover are treated separately to distinguish between atmospheric heat exchanges and the sensible heat input from the river discharge. The ice cover is assumed to be uniform in thickness, free of snow, and isothermal (or very nearly so) such that heat conduction within the ice is absent or negligible.

The Upper Surface Heat Balance

Atmospheric forcing on the upper surface of the ice cover can be written as:

$$\Sigma F = (1 - i_o)(1 - \alpha) F_r - \varepsilon_i \sigma T_o^4 + F_i + F_S + F_l \qquad (1)$$

where the right-hand side is, respectively, the absorbed shortwave radiation, the outgoing longwave radiation, the incoming longwave flux and the sensible and latent heat flux. At the onset of spring when solar radiation and air temperatures are increasing, the available energy increases the surface temperature, T_o to achieve thermal equilibrium with the atmosphere. Once the surface warms to the melting point, any additional energy becomes available for melting ice. The surface heat balance is then represented by the equation

$$\Sigma F = \begin{cases} 0 & \text{if} \quad T_o < 273 \text{ K} \\ -\rho_i L_f \, (dh/dt) & \text{when} \quad T_o = 273 \text{ K} \end{cases} \qquad (2)$$

Here, ρ_i is the ice density (900 kg/m^3), L_f the latent heat of fusion, h the ice thickness in meters, and t is the time in seconds.

The heat fluxes in equation 1 are based on the models and parameters of Maykut and Perovich, 1987 and the reader is referred to that paper for most of the details concerning the various treatments. All of the terms on the right-hand side of equation 1 except for the absorbed shortwave term are parameterized in terms of the surface temperature, T_o. The incoming shortwave radiation, F_r, is interpolated from the monthly averages given in Maykut and Untersteiner, 1971. Air temperatures for 1986 have been obtained at Tuktoyaktuk, NWT, located in the eastern portion of the delta and were smoothed to fit a sine function in the model. The albedo, α, is allowed to vary with ice thickness based on the empirical relationship given in Maykut and Untersteiner. Other variables required in the parameterization of the heat fluxes

included cloudiness, wind speed and relative humidity. These were taken from the June average values for the Mackenzie region given in *Climatic Atlas* (Brower, et. al.), 1988.

One aspect of the parameterization concerning the treatment of absorbed radiation will be mentioned here. Not all of the incoming shortwave radiation at the surface of the ice is immediately available for melting. Following Maykut and Perovich, a fraction of this energy (represented by $i_o F_r$) is transmitted through the ice layer with an exponential attenuation. The ice is thus partitioned into a surface layer of 10 cm where the absorbed shortwave energy is immediately available for melting and a lower layer where the remaining energy goes to internal melting rather than direct changes in ice thickness. Internal melting of sea ice increases the brine volume and consequently decreases the amount of energy required for mass changes. This is accounted for in the model by allowing the latent heat of fusion, L_f, to become a variable.

River Heat Flux

The heat supplied by the river discharge to the base of the ice cover is analogous to the oceanic heat flux included in most standard thermodynamic sea ice models. This is a poorly understood parameter and its value likely varies in space and time; most models assume a constant value between 0 and 10 W/m^2. The Maykut and Untersteiner results showed the equilibrium thickness of sea ice to be highly sensitive to this parameter, decreasing from about 6 meters to zero for a change in heat flux from 0 to 7 W/m^2. Utilizing the sequence of satellite images as well as the general features of the Mackenzie shelf morphology and river discharge, the basal heat flux will be explicitly parameterized in the development that follows.

As a simple and first approach, the river's effect on the ice cover is modeled as a convective heat flux analogous to the atmospheric sensible heat at the top surface of the ice. Convective heat flux is typically based on the bulk properties of the flow without including specific effects such as friction velocity, roughness length or the presence of a viscous sublayer for smooth flow. This is achieved by incorporating the various physical processes into a single convective heat transfer coefficient. Thus, the river heat flux at the base of the ice cover is represented by an equation of the form

$$R = f_{int}\, \rho_w\, c_p\, C_s\, u\, \Delta T \qquad (3)$$

where $\Delta T = (T_{plume} - T_{melt})$ is the difference between the bulk river plume temperature and the melting point (here 273 K) and

$$f_{int} = A_{plume}/A_{ice}$$

is the ratio of the plume's areal extent in contact with the ice cover to the total area of the ice cover. Also in equation (3), ρ_w = 1000 kg / m^3 is the density of water, c_p = 4200 J/(kgK), is the specific heat of water; u, the bulk plume speed and C_S is the heat transfer coefficient. Since the base of the ice cover is in equilibrium with the shelf water at the melting point, all of the available river energy goes to bottom ablation, i.e.,

$$dh_{base}/dt = -R/\rho_i L_f$$

River Parameters

Excepting ρ_w and c_p, the remaining four terms in equation (3) are not directly known. These terms are estimated, at least to within an order of magnitude, using geometrical arguments, imagery measurements and timing constraints on the breakup of the shelf ice. To begin estimating these parameters, an idealized geometrical representation of the shelf region will be employed. Figure 10 shows the study area with the model geometry. The shelf is represented by a cylindrical section with an inner radius of 30 km, outer radius of 90 km and an angular spread of 90 degrees. Because the fresh and relatively warm discharge is buoyant, the effective shelf depth will be less than the actual depth of about 10 m. Instead, an approximate mixing depth of 2 m is used, based on the salinity profiles and calculations of standing freshwater stock given in Macdonald and Carmack, 1991. With this geometry, the shelf coverage is roughly 5 x 10^9 m^2 with a total volume of 1 x 10^{10} m^3.

The discharge into the model region cannot be accurately known, since the published Canadian measurements (Water Survey of Canada 10LC014, 1986) are taken at Arctic Red River far upstream before the Mackenzie River separates into its various channels at the delta. It should be noted, however, that the majority of discharge (approx. 80%) occurs in the western portion of the delta (personal comm., 1993, S. Fafassnacht, Yellowknife, NWT and W. Hanna, Inuvik, Environment of Canada) where incidentally, the ice breakup is most dynamic as is apparent in Figures 3 and 4. With this information, the average discharge into the model region for the breakup period is approximately 2 x 10^4 m^3 s^{-1}.

Without a spatial and temporal series of salinity profiles in the shelf region, it is difficult to estimate the interaction dimension, f_{int}. However, this could be suggested by the residence time of the freshwater influx. Assuming the above values for discharge and shelf volume, the residence time for the freshwater in the model space is only 6 days. Since this is far shorter than the roughly 30 day melt period, the interaction dimension, f_{int} is taken to be unity, i.e., the plume is treated as if it were effectively in thermal contact with the entire ice cover as it flows out onto the shelf.

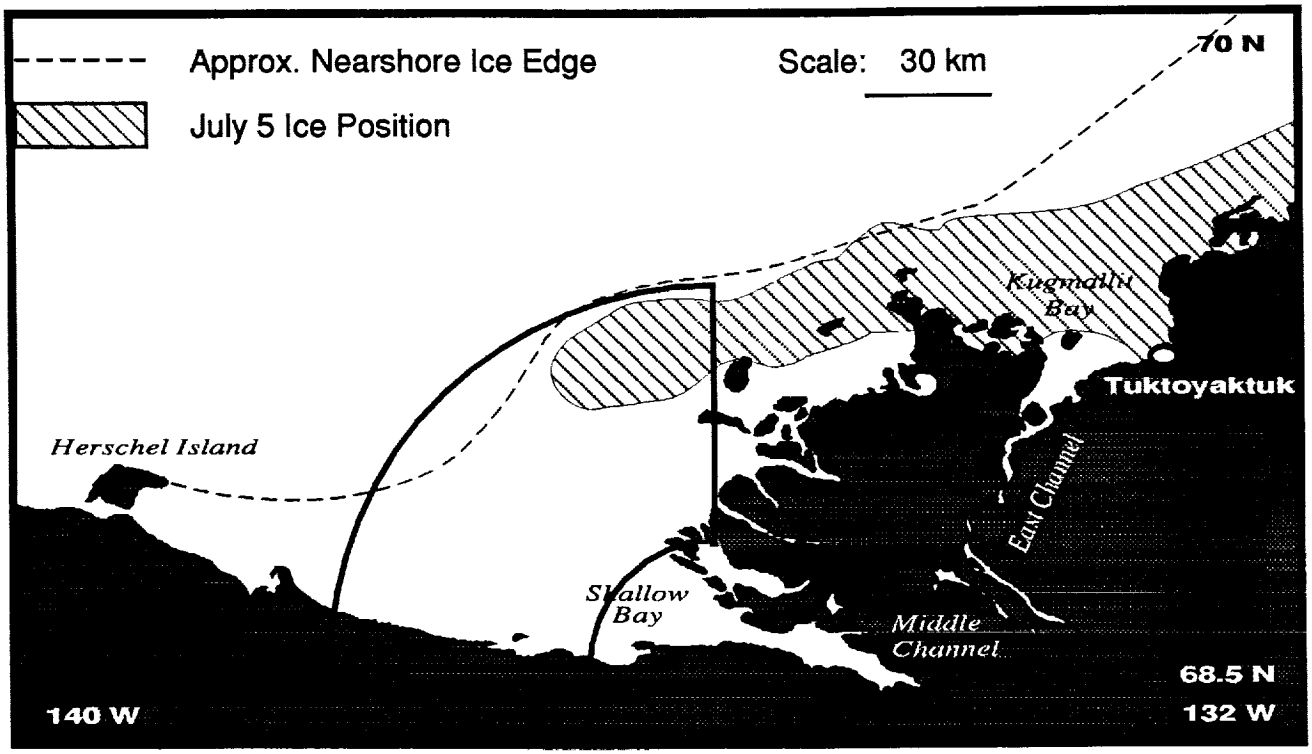

Figure 10. Schematic diagram of the idealized model region. Only the western portion of the delta is represented since these channels contain 80 percent of the Mackenzie River discharge. The bold cylindrical section has an inner radius of 30 km, outer radius of 90 km and an angular spread of 90 degrees. Shown for comparison is the limit of the fast ice (dashed line) and the extent of fast ice as of July 5 (hatched region).

The model shelf dimensions and discharge allow an estimation for the relative speed, u. The cross-sectional area receiving the freshwater input is 9.4×10^4 m^2. Assuming the velocity is constant with depth, the discharge enters the region with a speed of u_O = 0.2 m/s. Continuity requires this to fall off inversely with distance offshore as it radially spreads over the shelf. To avoid using spatially dependent quantities in the model, an averaged value over the shelf region will be employed. The quoted shelf dimensions give a geometrical average result of $0.55u_O$ such that the relative velocity taken in the model is of the order of 10^{-1} m/s.

The thermal forcing, ΔT, representing the temperature of the shelf water in contact with the ice cover is derived from the calibrated thermal infrared-band AVHRR images (such as in Figures 3 & 4). The distinct patches of open water adjacent to the delta establish initial temperature patterns as the river enters the model space. This surface temperature progress from 0°C just prior to the peak of discharge in early June to 10°C thirty days later when the delta is largely free of ice. Thus, the thermal forcing is given a temporal dependence as breakup progresses although, as in the other parameters, spatial patterns are ignored.

It should be pointed out, however, that the initial temperature adjacent to the coast should not be used for the thermal forcing. These measurements are taken before the river mixes with the shelf water, and the sensible heat will be overestimated if the thermal forcing is assumed equal to the river's input temperature. To account for this, mixing of the river discharge and shelf water is allowed with a specified ratio. The discharge represents a daily standing stock of freshwater of 0.25 meters when spread over the model region. If it is assumed, as previously, this mixes to a depth of 2 m, the ratio is then 1/8. Thus, in the model, the initial river temperature linearly increases over time at a rate of 10 K per 30 days but is cumulatively mixed with seven parts of shelf water at its previous temperature. This results in a slow exponential increase over time in the shelf water's temperature, although simply stated, the net effect is to reduce the thermal forcing rate derived from this to about half the river's warming rate, i.e., 5 K per 30 days. This warming rate appears to be reasonable based on satellite sea surface temperatures in 1986 and measured river water temperatures (Davies, 1975) although this observation must be taken cautiously since the values are derived from different years.

The last term to discuss is the (non-dimensional) heat transfer coefficient, C_S. Typically, given a melt rate, dh/dt, one arrives at this coefficient by measuring the bulk flow parameters, u and ΔT, and reversing equation (3) to solve for C_S. This method eliminates the need to estimate the heat flux from turbulent temperature and velocity fluctuations or from the mean temperature and velocity profiles. Josberger, 1987 presented such measurements from the 1983 Marginal Ice Zone Experiments (MIZEX) in the Bering Sea and Fram Strait by measuring the bottom ablation of ice floes advected into regions where they encountered higher relative ice-water speeds and ocean temperatures. His reported values of C_S showed little variation over a wide range of measured melt

rates, relative ice-water speeds and sea water temperature as well as for the two different locations. These values ranged from 2 x 10^{-4} to 8 x 10^{-4} and were even narrower (2 - 5 x 10^{-4}) for the Fram Strait measurements. One reason for the smaller range in the Fram Strait floes was attributed to the smoother ice pack. Increased fracturing and rafting of the Bering Sea ice creates a rougher surface and enhances turbulent transfer of heat to the ice. Since the near shore ice in the Mackenzie delta is likely to be relatively smooth this makes comparisons to the Fram Strait data more useful. The ice floes studied in the Fram Strait had horizontal dimensions of approximately 80 m and were exposed to relative ice-water speeds at the 2 m depth from 0.1 to 0.2 m/s and a thermal forcing of 2 to 5 K. These are very similar to the estimated parameters in this model and, as will be shown in the next section, a value of C_S = 1 x 10^{-4} gives the best results for the Mackenzie Delta ice.

RESULTS

Equation (1) is a fourth-order polynomial in the surface temperature, T_O and represents the energy gained at the top surface of the ice. At each time step the four (complex) roots of T_O are found and searched for a physically realistic solution whereupon T_O is updated until such a time occurs that it reaches the melting temperature. At this point energy gained at the surface becomes available for melting and the surface temperature is maintained at 273 K. The surface forcing terms all vary slowly over time and hence place no real constraints on the time step, *dt*. However, surface melting is assumed to take place in the upper 10 cm which requires the time step to be small enough such that melting greater than 10 cm does not occur over any one step. Here a time step of 0.5 days is used although there are no diurnal variations in any of the forcing.

Numerical simulations of the spring breakup period from May 25 (day 145) to July 14 (day 195), were run without a river component as a control case such that no basal heat flux was included. The equilibrium surface temperature on May 25 started at 269 K and did not reach the melting point until June 3 (day 154). Complete removal of the ice cover occurred on day 187 (July 6), requiring a total energy input of 5.4 x 10^8 J/m^2. The net atmospheric heat flux is shown with its various components in Figure 12. The ice decays in a parabolic form (see dashed line, Figure 11) in response to this nearly linear increase in the net surface flux.

Comparisons of ice decay were made to the Sachs Harbor, NWT data given by Bilello, 1980 where the average decay envelope for a 16 year period shows the onset of melting occurring about May 25 and completely decaying around July 10. The data suggested an empirical relationship for ice decay based on the accumulated thawing degree-days obtained by summing the daily difference between positive mean air temperatures and the melting temperature. Using this relationship with the Tuktoyaktuk air temperatures used in the present model, the predicted removal of a two meter ice cover occurs by day 190, in good agreement with the numerical simulation result

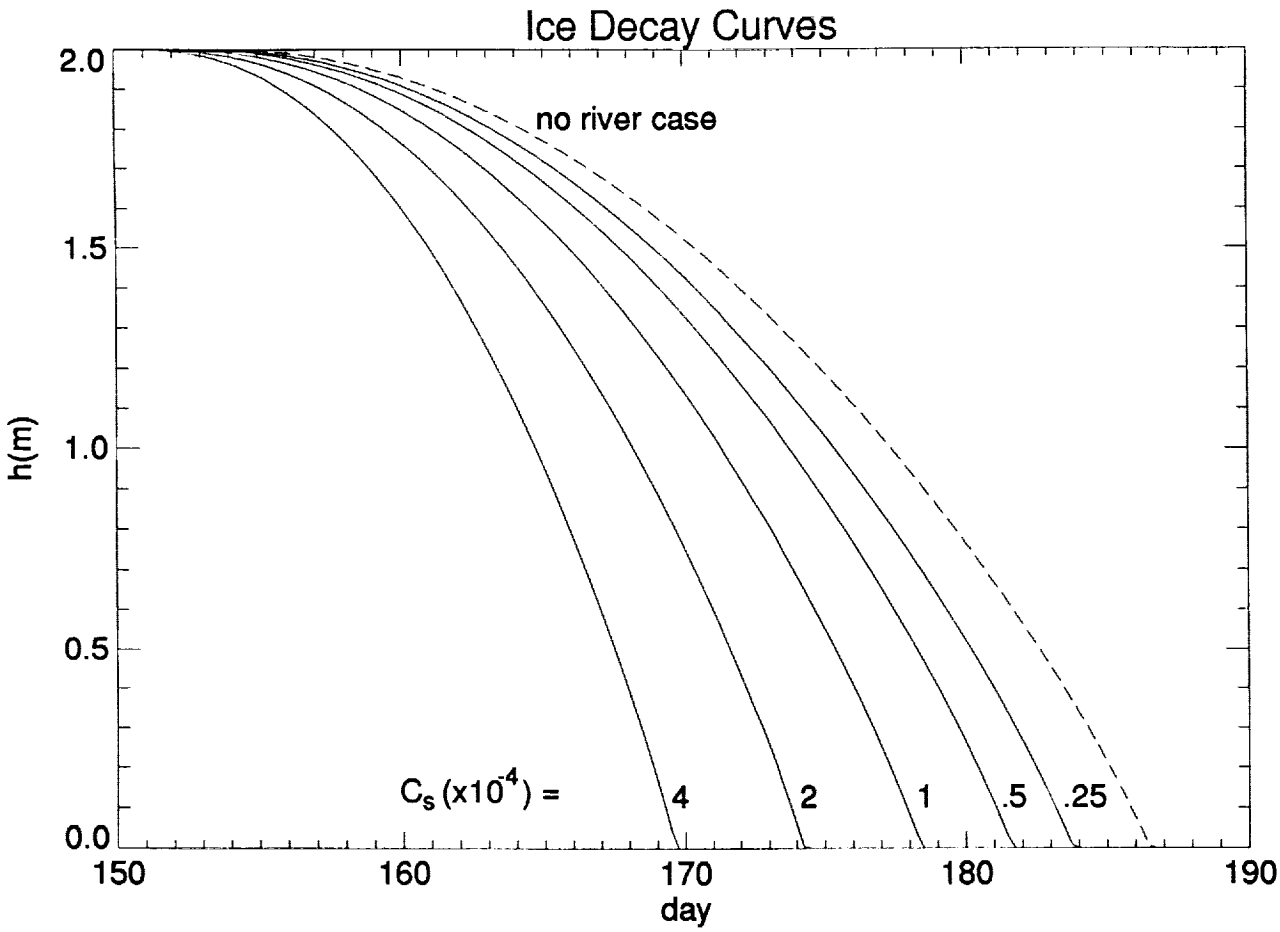

Figure 11. Ice decay curves depict the simulated results of melting due to atmospheric forcing and river heat. The dashed line is the limiting case of no basal heat flux (i.e. no river term) while the solid curves result from varying the river's heat transfer coefficient, C_s, from0.25×10^{-4} to 4×10^{-4}.

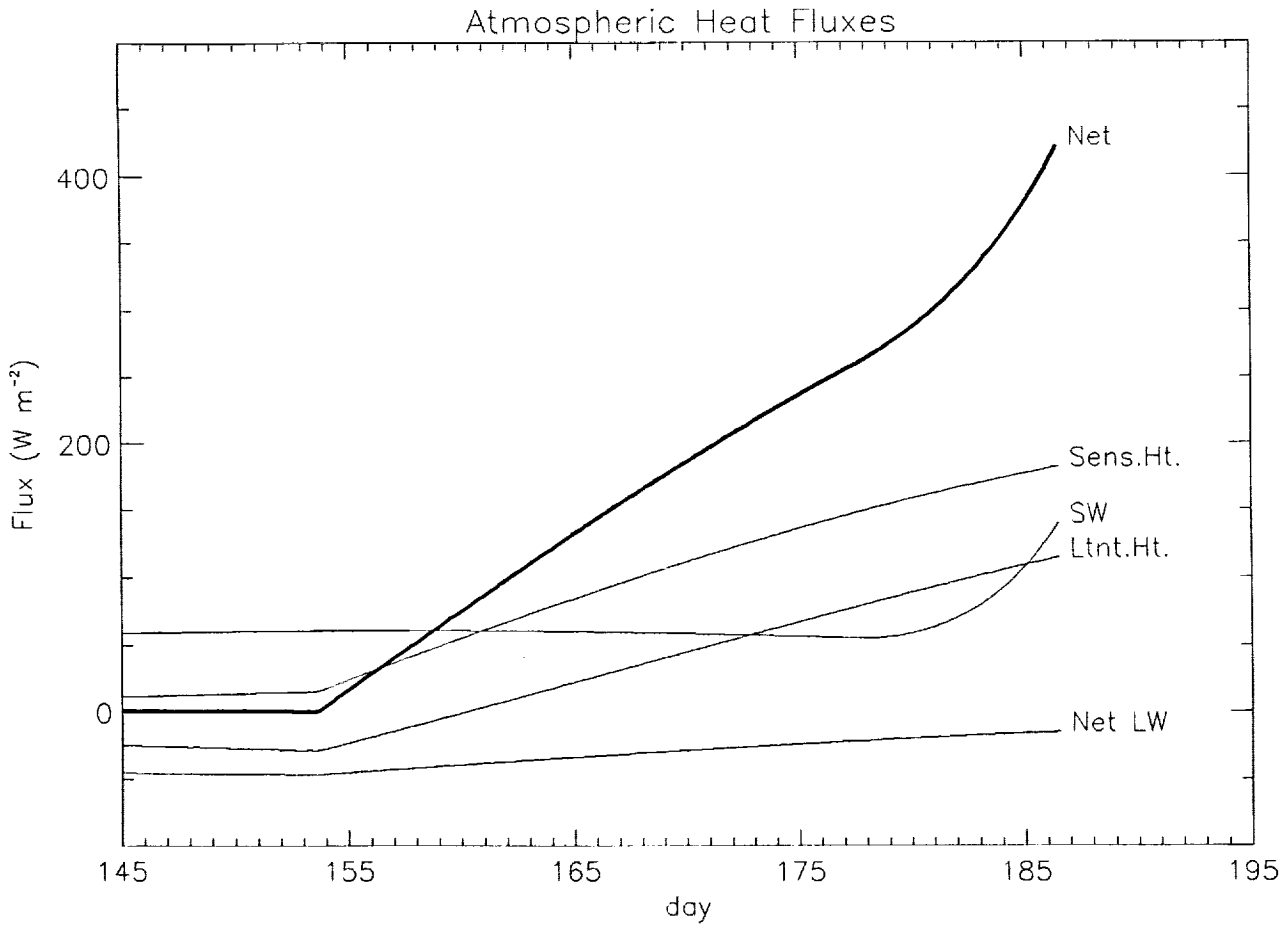

Figure 12. Atmospheric heat fluxes show forcing at the upper surface of the ice cover during the breakup period. Represented are the sensible heat, the absorbed shortwave radiation, the latent heat and the net longwave flux. The net atmospheric flux is shown in the bold line.

of day 187 and emphasizing the importance of the sensible heat flux in the surface balance of coastal regions.

Numerical simulations of the influence of the river include the previously described basal heat flux where the water temperature was "turned on" on June 1 (day 151) at the peak of discharge. Several simulations were run allowing for the heat transfer coefficient to assume values between 0.25×10^{-4} and 4×10^{-4}. The ice decay curves for these simulations are represented as solid lines in Figure 11 and, for comparison, the decay curve for no river discharge is represented by the dashed line in Figure 11. The results of these simulations were compared to the date of the break-up derived from the 1986 sequence of satellite images. The images show that all of the fast ice broke into floes by June 29 (day 180) which corresponds to a heat transfer coefficient of $C_S = 1 \times 10^{-4}$ (Figure 11). The river heat flux with this coefficient is shown along with the net atmosphere flux in Figure 13. Integrating these two curves gives the relative contribution from the two heat sources resulting in 58% atmospheric and 42% river.

In parameterizing the various river terms, no errors associated with them are given since most of the arguments are "order-of-magnitude" necessitated by the available data. Sensitivity to changes in the magnitude of any of the river parameters such as the heat transfer coefficient (C_s), the bulk plume speed (u), the fractional plume coverage (f_{int}) or the thermal forcing (ΔT) is suggested by the family of curves in Figure 11. Since the river heat flux responds linearly to these terms, a single change to any one of them will have the same result on the energy supplied by the river and the data of breakup. For instance, an increase in any one parameter by a factor of two results in breakup about four days earlier. The fraction of energy supplied by the river as a function of changes to one of these terms (e.g., C_s) is shown in Figure 14 where a non-linear dependence is apparent.

A different sensitivity occurs as a result of the initial date the thermal forcing ΔT is "turned on." Since the warming rate of the river water is linear, changing the starting date results in proportional changes to the amount of energy supplied by the river over the breakup period. Here, an earlier warming of the river by one week removes the ice cover approximately three days earlier as shown in Figure 15. The resulting fraction of energy supplied by the river in this case is plotted in Figure 16 where a linear dependence is apparent.

CONCLUSION

The modeling approach is necessarily simplistic given the nature of the problem and the lack of quantitative data in the water column. Spatial variability and a realistic mixed layer model for the shelf water was ignored. Also, only the spring melt period has been addressed in the present investigation. However, this approach highlights the key elements of the river discharge

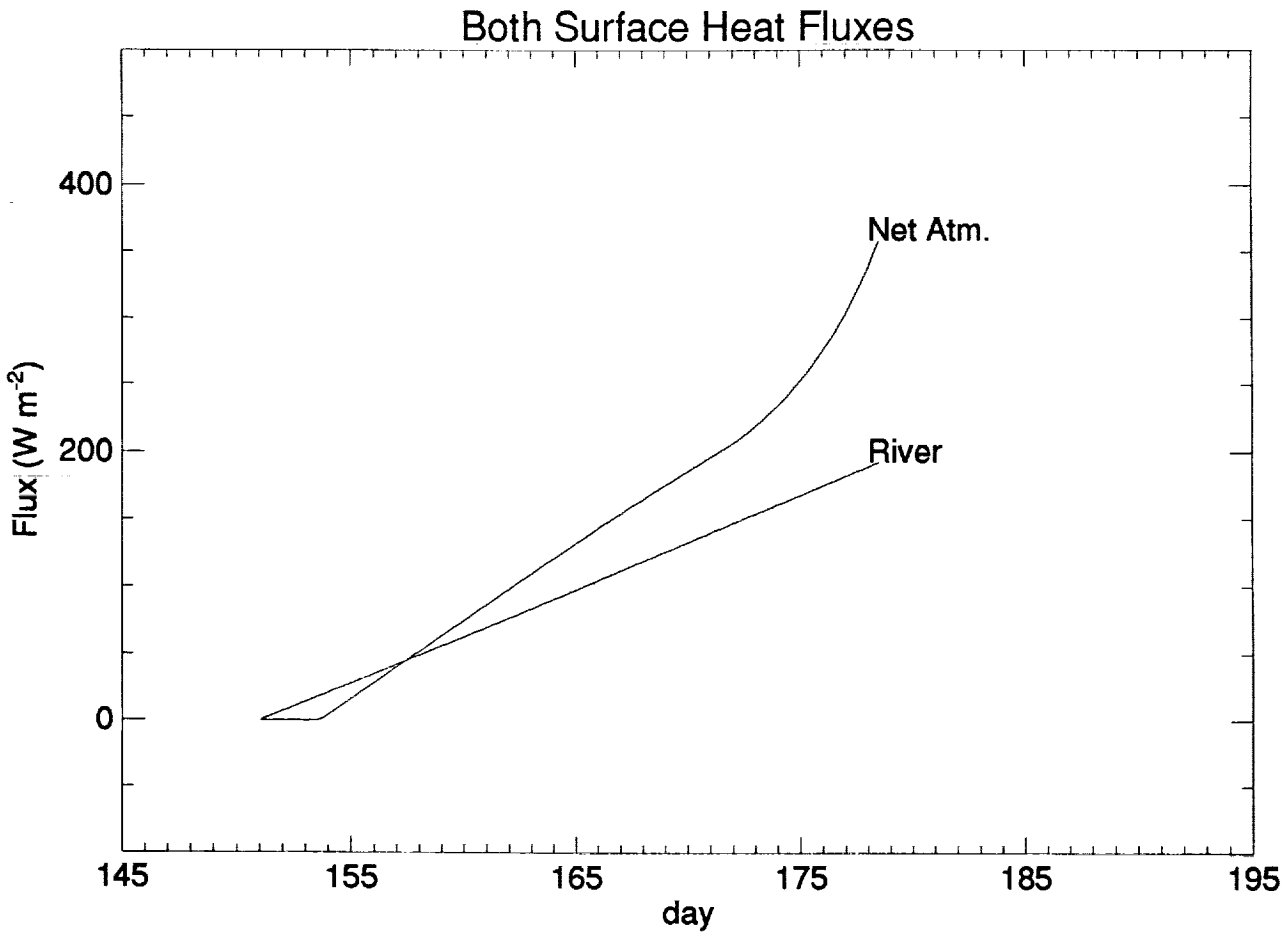

Figure 13. A comparison of the net heat flux on both the upper and lower surfaces of the ice cover. The net atmospheric flux is from figure 12 while the river flux corresponds a heat transfer coefficient of $C_s = 1 \times 10^{-4}$. Integrating these curves gives the relative contribution to melting from each surface with the result here of 52% atmospheric and 42% river melting.

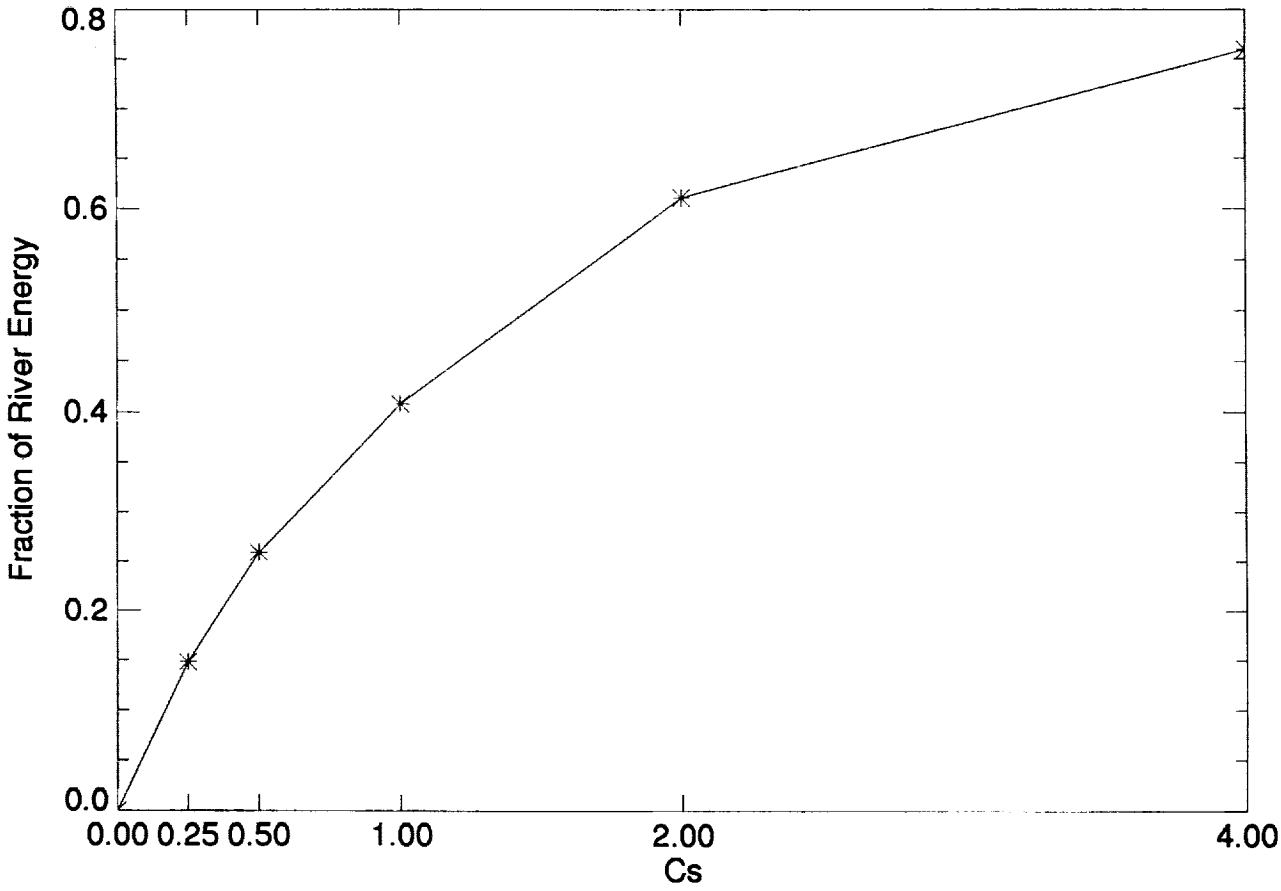

Figure 14. The river fraction of total energy used to melt the ice cover as a function of the heat transfer coefficient, C_s. The effect on the energy partition is non-linear and, since the river parameterization in the model responds proportionally to all of the constant terms (u, f_{int}, ΔT), a similar change to any single parameter will have the same effect on the energy partition.

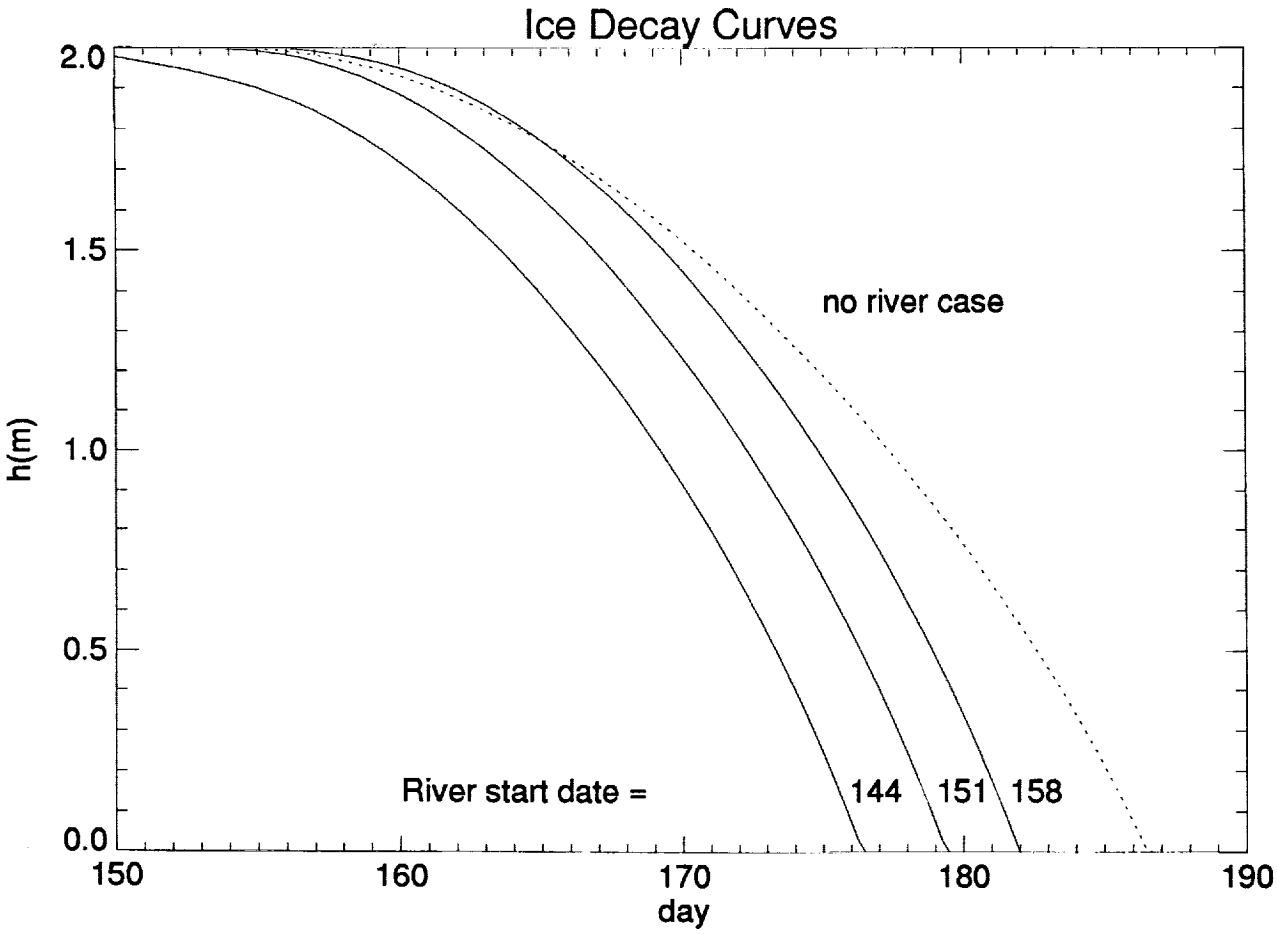

Figure 15. Influence of river discharge on the ice decay as a function of one week variations in the date the river heat "turns on". The most typical date that the river "turns on" is 151 with a heat transfer coefficient of $C_s = 1 \times 10^{-4}$

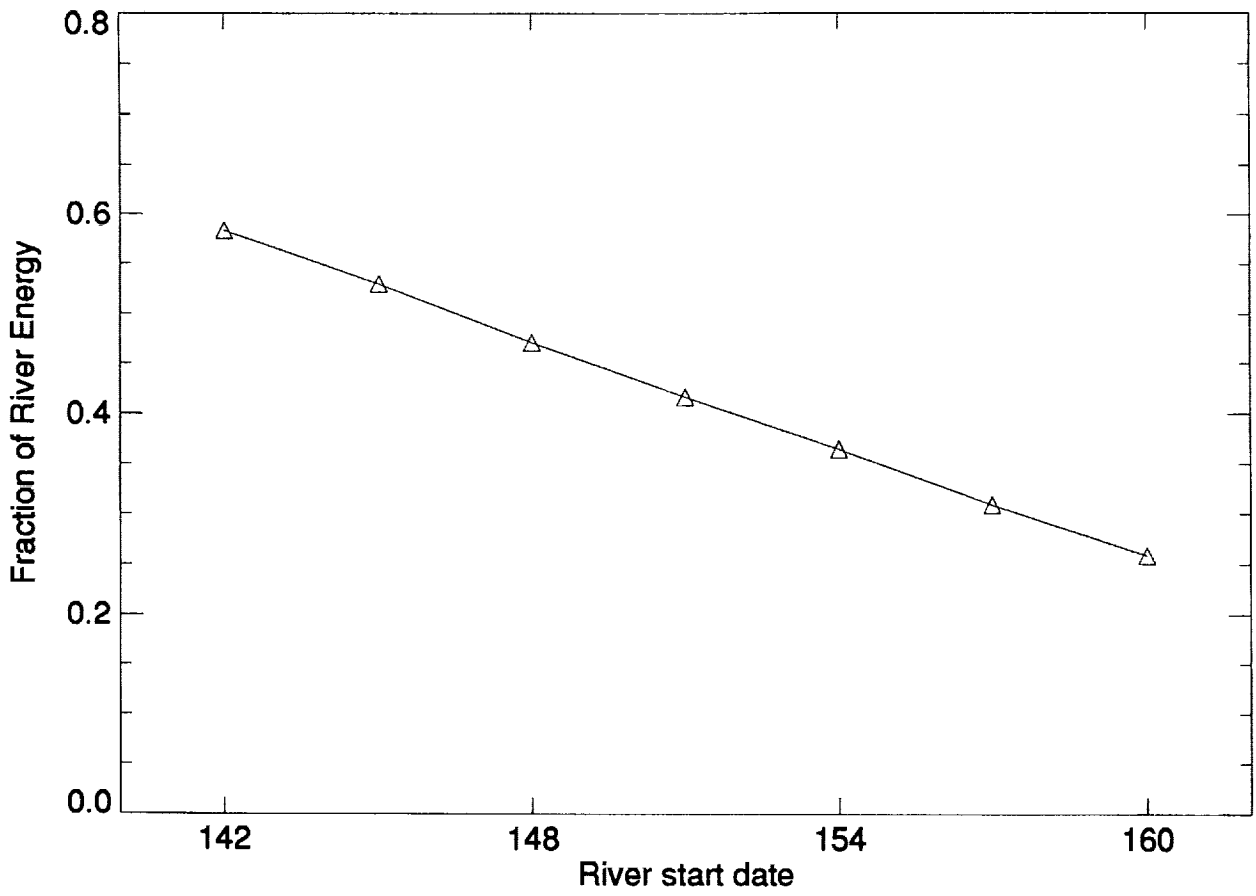

Figure 16. The river fraction of total energy used to melt the ice cover as a function of the date the river thermal forcing, ΔT, is "turned on". The effect here is linear since ΔT is itself linear in time and changing this date results in proportional changes to the total energy supplied by the river represented by the area under the curve in figure 13.

that influence sea ice and include the heat transfer coefficient (C_S), plume speed (u), fractional plume coverage (f_{int}), and thermal forcing (ΔT). Rivers do indeed supply a significant amount of sensible heat, accounting for approximately half of the energy required to melt the ice in the nearshore region. As a result, coastal areas receiving river discharge are free of ice conditions 10 to 14 days earlier, at a time when increasing air temperatures and solar radiation are available for the region's overall heat balance. Future modeling studies could begin to look at the annual energy balance and assess in a similar fashion the timing of freeze-up in the fall as well as feedback mechanisms related to the longer open water period in areas with river discharge.

ACKNOWLEDGMENTS

We thank the Polar Continental Shelf Project for providing accommodations and helicopter support, and the Water Survey of Canada, Inuvik for providing ice drilling equipment. We thank the Water Survey of Canada in Yellowknife for providing river discharge records and other very cordial assistance. Tom George provided aircraft support and assistance in aerial photography and video. Image processing was performed by Kristina Ahlnaes using the Interactive Image Analysis System at the Alaska SAR Facility and the University of Alaska, Alaska Data Visualization and Analysis Laboratory. This project was funded by NASA Grant NAGW 1835.

REFERENCES

Aagaard, K, 1984: The Beaufort Undercurrent, in *The Alaska Beaufort Sea: Ecosystems and Environments*, edited by P. W. Barnes, D. M. Shell, and E. Reimnitz. Academic, San Diego, Calif. 47-71.

Aagaard, K and L.K. Coachman. 1975: Toward an Ice-Free Arctic Ocean EOS 56 484--486

Barnes, P.W., and E. Reimnitz, 1976: Flooding of Sea Ice by the Rivers of Northern Alaska. Geological Survey Professional Paper 929, Richard S. Williams, JR. and William D. Carter, Editors, U.S. Government Printing Office, Washington, D.C. pp. 356-359.

Bilello, M., 1980: Decay Patterns of Fast Ice in Canada and Alaska. In "Sea Ice Processes and Models, Proc. of the AIDJEX International Commission on Snow and Ice Symposium," R. Pritchard, editor.

Brower, W.A., R. G. Baldwin, C. N. Williams Jr., J. L. Wise and L. D. Leslie 1988: Climatic Atlas of the Outer Continental Shelf Waters and the Coastal Regions of Alaska, Vol III, Chukchi and Beaufort Seas Department of Defense Document, NAVAIR 50--1C-553

Carmack, E.C., Macdonald, R.W. and Papadakis J.E. 1989: Water Mass Structure and Boundaries in the Mackenzie Shelf Estuary. *J. Geophys. Res., 94*(C12), pp. 18,043-18,055.

Davies, K.F., 1975: Mackenzie River Input to the Beaufort Sea, Beaufort Sea Technical Report #15, Water Survey of Canada, Department of the Environment of Canada, Clennan Square, 110-11 Ave. S. W., Calgary, Alberta T2R OB8, 72 pp.

Dean, K G., W.J.. Stringer, K. Ahlnaes, S.C. Searcy, T. Weingartner, (In press) The Influence of River Discharge on the Thawing of Sea Ice: Mackenzie River Delta, submitted to Polar Research, Norweign Polar Res. Inst., Oslo, Norway.

Hakkinen, S., 1986: Coupled Ice-Ocean Dynamics in the Marginal Ice Zones: Upwelling/Downwelling and Eddy Generation, *J. Geophys. Res.*, 91, C1, pp. 819-832.

Johannessen, O.M., J.A. Johannessen, E. Svendsen, R.A. Shuchman, W.J. Campbell and E. Josberger, 1987: Ice-Edge Eddies in the Fram Strait Marginal Ice Zone, Science, April, pp. 427 - 429.

Josberger E.G., 1987: Bottom Ablation and Heat Transfer Coefficients From the 1983 Marginal Ice Zone Experiments *J. Geophys. Res.* 92 (C7),pp. 7012-7016.

Kidwell, K.B. (ed.) 1991: NOAA Polar User Guide (TIROS-N, NOAA 6, NOAA 7, NOAA 8, NOAA 9, NOAA 10, NOAA 11, and NOAA 12), National Oceanic and Atmospheric Administration, National Environmental Satellite, Data, and Information Service, National Climatic Data Center, Satellite Data Services Division, Princeton Executive Square, Rm. 100, Washington D.C. 20233, p. 3-14 - 3-19.

Kovacs, A. and Mellor, M. 1974: Sea Ice Morphology in *The Coast and Shelf of the Beaufort Sea*. Published by the Arctic Institute of North America, John C. Reed and John E. Sater, editors, p. 113 - 161.

Newton J.L. 1973: The Canadian Basin: Mean circulation and intermediate scale flow features, Ph.D. thesis. Univ. of Washington, Seattle Washington, USA. 158 pp.

Macdonald, R.W. and Carmack, E.C. 1991: The Role of Large-Scale Under-Ice Topography in Separating Estuary and Ocean on an Arctic Shelf. *Atmosphere-Ocean, 29*(1), p. 37-53.

Macdonald, R.W., Carmack, E.C., McLaughlin, F.A., Iseki, K., Macdonald, D.M. and M.C. O'Brien, 1989: Composition and Modification of Water Masses in the Mackenzie Shelf Estuary, *J. Geophys. Res., 94(*C12), 18,057-18,070.

Marsh, P. and Hey, M. 1989: The Flooding Hydrology of Mackenzie Delta Lakes near Inuvik, N. W. T., Canada. *Arctic, 42*(1). 41-49.

Matthews, J.B. and W.J. Stringer, 1984: Spring break-up and flushing of an Arctic lagoon estuary. J. Geophys. Res., 89(C2), 2073-2079.

Maykut G.A. and D.K. Perovich, 1987: The Role of Shortwave Radiation in the Summer Decay of a Sea Ice Cover Journal of Geophysical Research 92 C7 7032--7044.

Maykut G.A. and N. Untersteiner, 1971: Some Results From a Time Dependent, Thermodynamic Model of Sea Ice, *J. Geophys. Res.* 76, pp. 1550-1575.

Micklin P., 1981: A Preliminary Systems Analysis of Proposed Soviet River Diversions on Arctic Sea Ice EOS 62 19 489.

Milliman, J.D. and Meade, R.H. 1983: World-wide delivery of sediments to the oceans. J. Geol., 91, pp. 1-21.

Morris , K., 1993: Annually recurring sea ice patterns in the nearshore region of the eastern Beaufort Sea as determined from satellite data (1974-1986), MS Thesis Univer. of Alaska Fairbanks, V. 1 & 2, 592 pp.

Planet, W.G.(ed.) 1988: Data Extraction and Calibration of TIROS-N/NOAA Radiometers, NOAA Tech. Memo. NESS 107 - Rev. 1, National Climatic Data Center, Satellite Data Services Division, Princeton Executive Square, Rm. 100, Washington D.C. 20233, 58 p. + appendices.

Reimnitz, E., C. Roderick, and S. Wolf, 1974: Strudel Scour: A Unique Arctic Marine Geologic Phenomenon, *J. Sed. Pet., 44(*2), 409-420.

UNESCO (United Nations Education, Scientific, and Cultural Organization) 1978: World water balance and water resources of the Earth, Stud. and Rep. in Hydrol. 25, Paris, France.

Semtner, Jr., A.J., 1984: The Climatic Response of the Arctic Ocean to Soviet River Diversions. *Climatic Change, 6*,, pp. 109-130.

Stirling I. and Cleator H. (eds), 1981: Polynyas in the Canadian Arctic, Environment Canada, Occasional Paper No. 45. Canadian Wildlife Service, Edmonton, Alberta, Canada T5K2J5. 72 pp.

Stringer W.J., 1988: The timing of snow melt flooding of Alaskan major North Slope rivers - An anomalous occurrence, in preparation, 32 pp.,

WMO (World Meteorological Organization) 1970: WMO Sea-Ice Nomenclature. WMO No. 259. TP 145, Secretariat of the World Meteorological Organization, Geneva, Switzerland. 147 pp.

Stringer, W.J., 1992; Use of Satellite Imagery to Determine the Timing of Springtime Seasonal Milestones associated with an Arctic River. Submitted to Photogrametric Engineering and Remote Sensing.

FIGURE CAPTIONS

Figure 1. Location Diagram of the Mackenzie River delta and vicinity.

Figure 2. AVHRR satellite images recorded on 17 April 1986 (left column) and 25 May 1986 (right column). The top images are color composites using the visible (B1), near-infrared (B2) and thermal infrared (B4) bands of data. The center images are visible band data that have been color coded to show albedo. The bottom images are the thermal infrared band data that have been color coded to show temperatures.

Figure 3. AVHRR satellite images recorded on 4 June 1986 (left column) and 14 June 1986 (right column). The top images are color composites using the visible (B1), near-infrared (B2) and thermal infrared (B4) bands of data. The center images are the visible band data that have been color coded to show albedo. The bottom images are the thermal band data that have been color coded to show temperatures.

Figure 4. AVHRR satellite images recorded on 12 July 1986 (left column) and 16 August 1986 (right column). The top images are color composites using the visible (B1), near-infrared (B2) and thermal infrared (B4) bands of data. The center images are the visible band data that have been color coded to show albedo. The bottom images are the thermal band data that have been color coded to show temperatures.

Figure 5. Location diagram of field sample sites.

Figure 6. Schematic diagram showing results of field observations and measurements.

Figure 7. Schematic diagram of the Mackenzie Delta region derived from the 1986 visible band images. This sequence depicts the development of the polynya system separating the fast ice from the pack ice as well as the river-induced melting immediately adjacent to the coast. The period represented is spring breakup with the image scenes beginning on May 25 (day 145) to July 5 (day 186).

Figure 8. Average albedo measurements for the regions defined in the schematic (upper figure) for the visible (lower left) and near infrared (lower right) bands. The Delta ice region is consistently lower in albedo and hence absorbs more shortwave radiation than other coastal areas.

Figure 9. Comparison of 1986 Mackenzie River discharge to areal calculations of river-induced open water. The dashed line is the discharge curve (m3 2-1) while the data points are a measurement of the overflow or open water areas (km2) immediately adjacent to the coast. The area of open water is derived from digitally processed AVHRR satellite images. The first three data points follow the discharge and for the most part represent overflows on top of the ice while the later points diverge as the area of open water enlarges as the ice cover recedes from the coastline.

Figure 10. Schematic diagram of the idealized model region. Only the western portion of the delta is represented since these channels contain 80 percent of the Mackenzie River discharge. The bold cylindrical section has an inner radius of 30 km, outer radius of 90 km and an angular spread of 90 degrees. Shown for comparison is the limit of the fast ice (dashed line) and the extent of fast ice as of 5 July 1986 (hatched region).

Figure 11. Ice decay curves depict the simulated results of melting due to atmospheric forcing and river heat. The dashed line is the limiting case of no basal heat flux (i.e. no river term) while the solid curves result from varying the river's heat transfer coefficient, C_S, from 0.25×10^{-4} to 4×10^{-4}.

Figure 12. Atmospheric heat fluxes show forcing at the upper surface of the ice cover during the breakup period. Represented are the sensible heat, the absorbed shortwave radiation, the latent heat and the net longwave flux. The overall net flux is shown in the bold line.

Figure 13. A comparison of the net heat flux on both the upper and lower horizontal surfaces of the ice cover. The net atmospheric flux (dashed line) is from figure 12 while the river flux corresponds to a heat transfer coefficient of $C_S = 1 \times 10^{-4}$. Integrating these curves gives the fractional contribution from each surface with the result here of 52% atmospheric and 42% river melting.

Figure 14. The river fraction of total energy used to melt the ice cover as a function of the heat transfer coefficient, C_S. The effect on the energy partition is non-linear and, since the river parameterization in the model responds proportionally to all of the constant terms $(u, f_{int}, \Delta T)$, a similar change to any single parameter will have the same effect on the energy partition.

Figure 15. Influence of river discharge on ice decay as a function of one week variation in the date that the river "turns on." The most typical date that the river "turns on" in the model is 151 with a heat transfer coefficient of $C_S = 1 \times 10^{-4}$.

Figure 16. The river fraction of total energy used to melt the ice cover as a function of the date the river thermal forcing, ΔT, is "turned on". The effect here is linear since ΔT is itself linear in time and changing this date results in proportional changes to the total energy supplied by the river represented by the area under the curve in Figure 13.

Appendix A:

List of Low Cloud-cover Images of the Mackenzie River Delta, 1986

DATE	ORBIT	SAT	BANDS	COMMENTS	Good Image for animation	10 Bit Data Ordered
April, 1986						
4/17/86	6933	N-9				XXX
MAY, 1986						
5/13/86	7300	N-9	1	Delta cloudy, open outside fast ice		
5/14/86	7314	N-9	1	Delta cloudy, open outside fast ice		
5/22/86	7427	N-9	1	Delta cloudy, open outside fast ice		
5/24/86	7455	N-9	1	Delta cloudy, open outside fast ice		
5/25/86	7469	N-9	1	tiny dark spots along delta (bare land?)	X	XXX
5/27/86	7497	N-9	1	delta visible through haze		
5/28/86	7512	N-9	1			
5/29/86	*7526	N-9	1,4	delta visible -- good image	X	
5/30/86	*7534	N-9	4	delta recognizable, IR detail		
5/30/86	*7540	N-9	1, 4	good detail B1 - no detail B4	X	
5/31/86	*7548	N-9	4	slight details visible - good image		
5/31/86	7554	N-9	1			
				cannot recognize delta in B4-IR, everything		
				gray line until May 30 - 1300 GMT		
				* flooding starts		
JUNE,1986						
6/1/86	7568	N-9	1	no IR detail	X	
6/2/86	7582	N-9	1	B1 good	X	
6/3/86	7596	N-9	1, 4	B4 - bay visible but no open water		
6/4/86	7610	N-9	1	delta snowfree with fact ice and lead beyond	X	XXX
6/5/86	7624	N-9	1		X	
6/6/86	*7639	N-9	1	some haze - good image		
6/7/86	7653	N-9	1	good image	X	
6/8/86	*7667	N-9	1	good image	X	
6/9/86	*7681	N-9	1, 4	coastline vaguely visible but not open water -B4	X	
6/11/86	7709	N-9	1	good image	X	XXX
6/12/86	7723	N-9	1		X	
6/13/86	7737	N-9			X	
6/13/86	7738	N-9	1	good image	X	
6/14/86	**7751	N-9		good image	X	XXX
6/14/86	7752	N-9	1	good image	X	
6/15/86	7765	N-9				
6/15/86	7766	N-9	1	good image	X	

6/18/86	7808	n-9	1	good image	X	
6/19/86	7822	N-9		melting of shorefast ice at delta became extensive	X	
6/20/86	7836	N-9	1	Good image	X	
6/22/86	7864	N-9		melt pools extensive at delta	X	
6/28/86	7949	N-9				
6/29/86	7963	N-9		Good image	X	
JULY, 1986						
7/3/86	*8019	N-9	1	shorefast ice is outside delta (gone?)	X	XXX
7/3/86	8020	N-9		good image	X	
7/5/86	*8047	N-9		melt tongues cut into shorefast ice	X	XXX
7/6/86	*8061	N-9			X	
7/6/86	8062	N-9	1	good image	X	
7/7/86	8076	N-9		melt tongues cut into ice obvious - ice is offshore	X	
7/8/86	8090	N-9			X	
7/9/86	8104	N-9			X	
7/12/86	8146	N-9			X	XXX
7/13/86	8160	N-9		some clouds	X	
7/14/86	8175	N-9		partly cloudy		
7/15/86	**8188	N-9			X	
7/17/86	8217	N-9			X	
7/19/86	8245	N-9		cloudy		
7/21/86	8273	N-9	1			
7/22/86	8287	N-9			X	
7/23/86	***8302	N-9		water at delta completely open		
7/24/86	8316	N-9				
				*melt tongues cut into shorefast ice		
				**on the 15th the distinct tongues have melted		
				laterally -- now a large indentation is evident		
				***end of melt sequence		
AUGUST, 1986						
8/1/86	8428	N-9	1	delta mainly cloudy		
8/2/86	8442	N-9		delta mainly cloudy		

8/3/86	8456	N-9		delta mainly cloudy		
8/4/86	8470	N-9		partly cloudy - ice is offshore		
8/5/86	8485	N-9		partly cloudy - ice is offshore		
8/7/86	8513	N-9		partly cloudy - ice is offshore		
8/8/86	8527	N-9		partly cloudy - ice is offshore	X	XXX
8/11/86	8569	N-9	1, 4	partly cloudy - ice is offshore - IR shows land		
8/12/86	8583	N-9		partly cloudy - ice is offshore		
8/14/86	8612	N-9	1, 4	partly cloudy - ice is offshore		
8/15/86	8626	N-9	1, 4	partly cloudy - ice is offshore		
8/16/86	*8634	N-9	4	good image - land colder than water, almost clear		
8/16/86	*8640	N-9	1	cloud-free, ice is offshore	X	XXX
8/18/86	8668	N-9	1	delta cloudy		
8/19/86	8682	N-9	1, 4			
8/24/86	8747	N-9	4	Mackenzie River warmer than the land		
8/25/86	8762	N-9		Mackenzie River warmer than the land		
8/26/86	8781	N-9	1, 4		X	XXX
8/27/86	8795	N-9	1, 4	delta cloudy		
8/28/86	8809	N-9	1, 4	delta cloudy		
8/30/86	8832	N-9	4			
8/31/86	8846	N-9	4	river visible		
8/31/86	8851	N-9	1, 4			
8/31/86	8852	N-9	1, 4			
				* night thermal		
SEPTEMBER, 1986						
9/1/86	8866	N-9	1, 4			
9/2/86	8874	N-9	4	river clear - delta partly sunny		
9/2/86	8880	N-9	1, 4	river clear - delta partly sunny -land warm, can't see river		
9/3/86	8894	N-9	1, 4			
9/4/86	8908	N-9	1, 4	delta clear		
9/5/86	8922	N-9		delta clear		
9/6/86	8936	N-9	4	delta clear		XXX
9/7/86	8950	N-9	1, 4	delta clear		
9/8/86	8959	N-9	4	delta clear - can almost guess ice edge		
9/8/86	8964	N-9	1	delta clear		XXX
9/10/86	8993	N-9	1	delta clear		
9/11/86	9007	N-9	1	delta clear		

9/14/86	9049	N-9	1, 4	delta clear - night pass also clear		XXX
9/19/86	9120	N-9	1, 4	partly cloudy		
9/20/86	9134	N-9	1, 4	partly cloudy		
9/22/86	9157	N-9	4	mostly sunny		
9/25/86	9205	N-9	1, 4	mostly sunny		
9/26/86	9213	N-9	4	mostly sunny		
9/27/86	9227	N-9	4	partly sunny		
9/30/86	9275	N-9	1, 4	partly sunny		
9/30/86	9275	N-9	1, 4	partly sunny		
10/1/86	9283	N-9	4	river dark - land light		
10/3/86	9312	N-9	4			
10/3/86	229	N-10				
10/6/86	9359	N-9				XXX
10/7/86	285	N-10				
10/9/86	9396	N-9				
10/15/86	399	N-10		aloudy along coast with open water		
10/17/86	428	N-10		good image		
10/19/86	448	N-10				
10/21/86	485	N-10		sea ice almost shorefast, river arms in delta open (?)		
10/22/86	490	N-10				
10/24/86	528	N-10		river frozen (?)		
10/26/86	9642	N-9		river still open?		
10/27/86	9650	N-9				
10/27/86	9655	N-9				
10/27/86	9656	N-9		freezeup begins?		
10/28/86	9664	N-9		delta looks frozen		
10/31/86	9712	N-9		delta looks frozen with overflow		
1991	AVHRR and Landsat Data					
5/4/91	24037	N-10		Mackenzie Delta area clear.		XXX
5/13/91	13563	N-11		Mackenzie Delta area clear but some haze in Banks Is. area.		XXX
5/13/91				Landsat TM Scene Number 5266620032		XXX

				*rivers definately open		
				** wind influence opens Mackenzie lead		

Appendix B:

River/Sea-Ice Model Code

The river-sea ice model code was written in PV-WAVE command language syntax. PV-WAVE is a software system for the analysis of scientific and technical data, a programming language, and a plotting and image display package. It is available through Precision Visuals, Incorporated, Boulder Colorado. Another compatible software system is IDL/IMSL to which this code should be portable but has not been attempted.

ICEMODEL.PRO

```
pro icemodel, dt_day=dt_day,alpha=alpha,csi=csi,river=river,print=print, $
  rdate=rdate
common plotstuff,day,h_ice,shortwave,albedo,lw_in,lw_out,sens_heat,$
  ltnt_heat,rvr_heat,airtemp,ltnt_fusion,esat_air,esat_ice,$
  io,iday_melt,melt_srfc,melt_btm,day_start,day_int,n_step

;DEFINE TIME STEP UNITS IN DAYS:
if not keyword_set(dt_day) then dt_day = 0.25      ;day

sec_day = 24.*60.*60.
dt_sec = dt_day*sec_day                            ;sec

day_start = 145.
day_int = 50.
day_max = day_start + day_int

;ARRAY SIZE:
n_step = 1 + day_int/dt_day

;DEFINE THE TIME-DEPENDENT ARRAYS:
;-----------------------------------------------------------------
day = day_start + dt_day*findgen(n_step)
h_ice = fltarr(n_step)        ;ice thickness,  m
shortwave = fltarr(n_step)    ;incoming SW,   W/m^2
albedo = fltarr(n_step)       ;surface albedo  non-dim.
lw_in = fltarr(n_step)        ;Incoming Longwave, W/m^2
lw_out = fltarr(n_step)       ;Outgoing Longwave,  W/m^2
sens_heat = fltarr(n_step)    ;Sensible heat flux, W/m^2
ltnt_heat = fltarr(n_step)    ;Latent heat flux, W/m^2
```

```
rvr_heat = fltarr(n_step)     ;Oceanic (river) flux,  W/m^2
airtemp = fltarr(n_step)      ;Air temps,  K
ltnt_fusion = fltarr(n_step) ;Latent heat of fusion, J/kg
esat_air = fltarr(n_step)     ;Air saturation vapor pressure, mbar
esat_ice = fltarr(n_step)     ;Ice sat. vapor pressure, mbar
;---------------------------------------------------------------


;INITIALIZE SOME CONSTANTS:
rho_ice = 900.                ;Ice density,  kg/m^3
rho_water = 1000.             ;Water density,  kg/m^3
cp = 4200.                    ;specific heat,  J/kg/K

stef_bltz = 5.67e-8           ;Stefan-Boltzman const, W/m^2/K^4

;SURFACE ABSORPTION AND INTERNAL MELT PARAMETERS:
io = 0.3                      ;Fraction transmitted
kappa = 1.5                   ;Extinction coefficient,  per meter
ho = 0.1                      ;Srfc melt layer thickness, m

ltnt_fusion(*) = 0.334e6      ;Latent heat of fusion,  J/kg

;INITIAL ICE THICKNESS:
h_ice(0) = 2.0                ;meter

;BOTTOM TEMPERATURE:
tbtm = 273.                   ;K

;OUTGOING LONGWAVE EMISSIVITY:
epsilon = 0.95

;DERIVED CONSTANTS:
rhol = rho_ice*ltnt_fusion(0)
rhoc = rho_ice*cp

;SINE-CURVE FIT TO AIRTEMP DATA
si= sin(2.*!pi*day/(365.) - 2.*!pi*121./365.)
airtemp = 273. + (-11. + 22.*si)
```

```
;+++++++++++++++    BEGIN DEFINING THE FLUXES:    ++++++++++++++++++++++

;INCOMING LONGWAVE:
;Maykut Parameterization:
cloud = 0.3     ;see CLIMATIC ATLAS
lw_in = (0.7855 + 0.2232*(cloud^2.75))*stef_bltz*(airtemp^4)

;SHORTWAVE INPUT (see Maykut)
sw_m = 0.3858*[0.,0.,100.,420.,730.,785.,575.,370.,155.,20.,0.,0.,0.]
;Julian date of each month:
month_day = [1.,32.,60.,91.,121.,152.,182.,213.,244.,274.,305.,335.,366.]
month_day = month_day + 15.
;interpolate to day array:
shortwave = spline(month_day,sw_m,day)

;ALBEDO:
if keyword_set(alpha) then begin
    ;Constant Albedo:
    albedo(*) = alpha
endif else begin
    ;Thickness dependent albedo (see Maukut)
    albedo(0) = 0.21 + 1.026*(h_ice(0) < 1.0) - 0.516*(h_ice(0) < 1.0)^2
endelse


;SENSIBLE HEAT PARAMETERS:
rho_air = 1.3                          ;air density            kg/m^3
cp_air = 1004.                         ;specific heat          J/kg/K
cs_sens = 1.75e-3                      ;bulk heat transfer coeff.
k_sens = rho_air*cp_air*cs_sens
wind_speed = 9.0                       ;m/sec  see Climatic Atlas
;sens_heat = surface temp dependent

;LATENT HEAT FLUX PARAMETERS:
ltnt_vap = 2.49e6                      ;latent ht of vapor.    J/kg
cs_ltnt = 1.75e-3                      ;ltnt bulk transfer coeff.
po = 1013.                             ;surface pressure       mbar
```

```
k_ltnt = 0.622*rho_air*ltnt_vap*cs_ltnt/po
rel_hum = 0.8                                   ;relative humidity

b1 = 2.7798202e-6                               ;see Maykut
b2 = -2.6913395e-3
b3 = 0.9792084
b4 = -158.63779
b5 = 9653.1925

esat_air = b1*airtemp^4 + b2*airtemp^3 + b3*airtemp^2 + b4*airtemp + b5
;esat_ice = surface temp dependent
;ltnt_heat = surface temp dependent

;RIVER FLUX:
ap2ai =1.0                                      ;ratio of plume area to ice area
if not keyword_set(csi) then csi = 2.0  ;non-dim. heat transfer coeff.
cs = csi*1.e-4
plume_speed = 0.1                               ;m/s
dtemp_dt = 10./30                               ;River input, Kelvin per day

;plume temperature = f(t)
;River tempertaure turned on day:
day_rvr_start = 151

n_zero = (day_rvr_start - day_start)/dt_day
dlta_temp_init = fltarr(n_step)
dlta_temp_init(0:n_zero) = 0.0
for i=n_zero+1,n_step-1 do $
     dlta_temp_init(i) = dtemp_dt*dt_day*float(i-n_zero)

dlta_temp_plume = 0.5*dlta_temp_init
if keyword_set(river) then $
     rvr_heat = ap2ai*rho_water*cs*cp*plume_speed*dlta_temp_plume


;++++++++++++++++++  BEGIN TIME INTEGRATION PROCESS:   +++++++++++++++++

;Coefficients for determing the roots of the surface heat balance equation:
```

```
aco = fltarr(5)
aco(2) = -k_ltnt*wind_speed*b3                          ;Tsrfc^2 term
aco(3) = -k_ltnt*wind_speed*b2                          ;Tsrfc^3 term
aco(4) = -epsilon*stef_bltz - k_ltnt*wind_speed*b1 ;Tsrfc^4 term

temp_srfc = 0.0
melt_srfc = 0.0
melt_btm = 0.0

imax = day_int/dt_day - 1
iday0 = imax

for iday = 0,imax do begin
    idaypl = iday+1

    ;CONSTANT COEFFICIENT TERM:
    aco(0) = shortwave(iday)*(1. - albedo(iday))*(1. - io) $
           + lw_in(iday)      $
           + k_sens*wind_speed*airtemp(iday)  $
           + k_ltnt*rel_hum*wind_speed*esat_air(iday) $
           - k_ltnt*wind_speed*b5
    aco(1) = -k_sens*wind_speed - k_ltnt*wind_speed*b4


    ;SOLVE FOR SURFACE TEMPERTURE:
    zroots,aco,root
    temp_real = float(root)
    temp_imag = imaginary(root)

    ;GET REAL ROOT AND SET TO 273 IF NECESSARY:
    for i=0,3 do begin
      if (temp_imag(i) eq 0.0 and temp_real(i) lt 300. $
          and temp_real(i) gt 200.) then temp_srfc = temp_real(i) < 273.
    endfor

    ;CALCULATE SURFACE DEPENDENT FLUXES:
    sens_heat(iday) = k_sens*wind_speed*(airtemp(iday) - temp_srfc)
    lw_out(iday) = epsilon*stef_bltz*temp_srfc^4
```

```
ltnt_heat(iday) =  k_ltnt*wind_speed*(rel_hum*esat_air(iday) -  $
 (b1*temp_srfc^4 + b2*temp_srfc^3 + b3*temp_srfc^2 + b4*temp_srfc + b5))


;HEAT FLUX TO SURFACE:
f_srfc =  shortwave(iday)*(1. - albedo(iday))*(1. - io) $
       + lw_in(iday)       $
       - lw_out(iday)      $
       + sens_heat(iday)     $
       + ltnt_heat(iday)


;CALCULATE AMOUNT OF SURFACE MELTING:
dh_srfc = -dt_sec*f_srfc/(rho_ice*ltnt_fusion(iday))
dh_srfc = (temp_srfc eq 273.)*dh_srfc
melt_srfc = melt_srfc - dh_srfc

;BOTTOM ABLATION:
f_btm = rvr_heat(iday)
dh_btm = -dt_sec*f_btm/(rho_ice*ltnt_fusion(iday))
melt_btm = melt_btm - dh_btm

;UPDATE THICKNESS:
h_ice(idayp1) = 0.0 > (h_ice(iday) + dh_srfc + dh_btm)
if (h_ice(idayp1) eq 0.0) then begin
    iday_melt=iday
    goto,melted
endif

;UPDATE THICKNESS-DEPENDENT ALBEDO:
if not keyword_set(alpha) then  $
albedo(idayp1) = 0.21 + 1.026*(h_ice(idayp1) < 1.0) $
               - 0.516*(h_ice(idayp1) < 1.0)^2


;UPDATE LATENT HEAT CHANGES:  ;See Maykut and Perovich
atten = io*(1.-albedo(iday))*(1. - exp(-kappa*(h_ice(iday)-ho)))
dldt = -atten*shortwave(iday)/(rho_ice*h_ice(iday))
```

```
    ltnt_fusion(idayp1) = ltnt_fusion(iday) + dt_sec*dldt

    ;CONTINUE TIME LOOP:
endfor

;EXIT TIME STEPPING LOOP:
melted:

openw,1,'h_ice.dat'
writeu,1,h_ice
close,1

return
end
```